

MASARYKOVA UNIVERZITA
PŘÍRODOVĚDECKÁ FAKULTA
ÚSTAV TEORETICKÉ FYZIKY A ASTROFYZIKY

Diplomová práce

BRNO 2016

BC. KLÁRA LOUKOTOVÁ

MASARYKOVA UNIVERZITA
PŘÍRODOVĚDECKÁ FAKULTA
ÚSTAV TEORETICKÉ FYZIKY A ASTROFYZIKY



Searching For Relic Radio Sources

VEDOUCÍ DIPLOMOVÉ PRÁCE: MGR. FILIP HROCH, PH.D.

Bibliografický záznam

Autor: Bc. Klára Loukotová
Přírodovědecká fakulta, Masarykova Univerzita
Ústav teoretické fyziky a astrofyziky

Název práce: Studium pozůstatků rádiových galaxií

Studijní program: Fyzika

Studijní obor: Teoretická fyzika a astrofyzika

Vedoucí práce: Mgr. Filip Hroch, Ph.D.

Akademický rok: 2015/2016

Počet stran: x + 58

Klíčová slova: radioastronomie, synchrotronové záření, pozůstatky
rádiových galaxií, CSS, LOFAR

Bibliographic Entry

Author: Bc. Klára Loukotová
Faculty of Science, Masaryk University
Department of Theoretical Physics and Astrophysics

Title of Thesis: Searching for relic radio sources

Degree of Programme: Physics

Field of Study: Theoretical Physics and Astrophysics

Supervisor: Mgr. Filip Hroch, Ph.D.

Academic Year: 2015/2016

Number of Pages: x + 58

Keywords: radio astronomy, non thermal radio continuum, radio relics, CSS, synchrotron radiation, radiative age, LOFAR

To everyone who believed in finishing of this thesis.

I declare that I have written my diploma thesis on my own and using exclusively the cited resources. I agree with lending of the thesis and making it public.

Brno, 5th January 2016

Klára Loukotová

Abstrakt:

V poslední době narůstá počet důkazů, že AGN aktivita, která je poháněna akrecí na supermasivní černou díru, může mít epizodický charakter. To, v jakých časových škálách takový cyklus probíhá, není stále zcela pochopeno. Porozumění tomuto jevu by mělo zásadní vliv na naše znalosti formování a vývoje galaxií, protože bychom byli schopni lépe odhadovat celkovou energii uvolněnou z AGN do mezihvězdné a meziglaktické látky. V překládané práci studuji spektra několika CSS zdrojů a pozůstatků po rádiových galaxiích. Pomocí modelů zářivého ochlazování odhaduji stáří těchto objektů. Část této práce je věnována úvodu do radioastronomie a jejím technikách a popisu synchrotronového záření.

Klíčová slova: radioastronomie, synchrotronové záření, pozůstatky radiových galaxií, zářivý věk, CSS, LOFAR

Abstract:

There has been a growing body of evidence that AGN activity, which is powered by mass accretion onto a super massive black hole could be episodic. But the activity duty cycle is not yet fully understood. Such a knowledge would be crucial for understanding the influence of AGN on galaxy formation and evolution since we would be able to constrain the total energy output by AGN in the ISM and IGM. In presented thesis we study the sample of compact steep spectrum sources and radio relics. Using the models of radiative cooling we estimate the radiative ages of the source. Part of this thesis is dedicated to setting a background in radio astronomy and its techniques and also to the description of synchrotron radiation.

Keywords: radio astronomy, non thermal radio continuum, radio relics, CSS, synchrotron radiation, radiative age, LOFAR



Masarykova univerzita

Přírodovědecká fakulta



ZADÁNÍ DIPLOMOVÉ PRÁCE

Student : Bc. Klára Loukotová, učo 358161

Studijní program : Fyzika

Studijní obor : Teoretická fyzika a astrofyzika

Ředitel Ústavu teoretické fyziky a astrofyziky PřF MU Vám ve smyslu Studijního a zkušebního řádu MU určuje diplomovou práci s tématem:

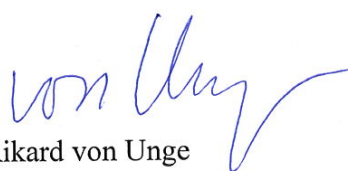
Searching for relic radio sources

Searching for relic radio sources


Zásady pro vypracování: Radio sources associated with elliptical galaxies are powered by active galactic nuclei via plasma jets. After this phase, the activity in the nuclei fades away. However, the radio lobes may still remain detectable for a long time if they are subject to radiative losses only. The presented theme is focused on searching for this kind of relic radio sources. The impossibility of observing full life-cycle of one single object is the crucial difficulty common to all fields of astronomy. Therefore one has to use indirect methods to determine the age and evolutionary stage of the source. In radioastronomy these methods are usually based on spectral indices at low frequencies and morphology of the radio emission. Available radio catalogues and radio surveys will be used to select candidates that are suitable for further studies using images obtained with LOFAR. The observations will be subject of statistics in order to draw a conclusion for evolution of the radio sources. Data of various radio and high-energy surveys as well as observations with LOFAR are expected to be used. Standard graduate-level statistical and physical methods are required.

Jazyk závěrečné práce : český, anglický nebo slovenský
Vedoucí diplomové práce : Mgr. Filip Hroch, Ph.D.
Datum zadání diplomové práce : prosinec 2015
Datum odevzdání diplomové práce : dle harmonogramu ak. roku 2015/2016

V Brně prosinec 2015


Rikard von Unge
ředitel ÚTFA

Zadání diplomové práce převzal dne: 1.12.2015


Podpis studenta

Contents

1	Introduction	1
1.1	Thesis outline	1
2	Radio astronomy	2
2.1	History of radio astronomy	2
2.2	Radio observation	4
2.3	Brightness temperature	6
2.4	Radio telescopes	7
2.5	The noise	10
2.6	Radio interferometry	11
2.7	Radio sky	14
3	Active galactic nuclei	16
3.1	AGN types	16
3.2	Unification of AGN species	18
3.3	Super massive black holes	19
4	Synchrotron emission	22
4.1	The beaming effect	23
4.2	Synchrotron power from a single electron	25
4.3	The spectral shape of synchrotron radiation	28
4.4	Self-absorbed synchrotron radiation	29
5	Inverse Compton scattering	32
5.1	Inverse Compton scattering on CMB photons	33
6	Spectral ageing	34
6.1	The model of an active phase	34

6.2	The compact steep-spectrum and gigahertz peaked-spectrum radio sources	37
6.3	Radiative ages of CSSs	38
7	Relic radio galaxies	42
7.1	Radio relic of young radio sources	42
7.2	Restarted sources	42
7.3	Fading relics	43
7.4	The model of dying radio source	44
7.5	The very steep spectrum radio sources	47
7.6	Fitting the observed data with the model	47
8	LOFAR	51
8.1	Technical details	51
8.2	LOFAR on radio relics	52
9	Conclusions	53
	Bibliography	54

Chapter 1

Itroduction

Since I had been working in high-energy astrophysics for my bachelor thesis I wanted to explore new field of astronomy. Radio band was an ideal candidate.

The phenomena I want to focus on is a relic radio galaxy. This poetic name represents a radio source in the last stage of its life when the activity in AGN centre has ceased. I would like to understand the mechanism of cooling of such a source. The cooling is realized namely by synchrotron radiation. I want to make a model both of active and relic phase of AGN cooling and apply them on a sample of sources trying to estimate their radiative ages.

1.1 Thesis outline

As part of working on this thesis I have tried to familiarize with radio astronomy and its techniques, entirely new field to me. This journey of mine is covered in chapter 2. Next step was to explore my objects of interest - active galactic nuclei (chapter 3) or more precisely relic radio galaxies (chapter 7). How we can obtain information about time scales of radio relics and AGN duty cycles from their spectra is discussed in chapters 6 and 7. These chapters cannot be understood without background in radiative processes, namely synchrotron radiation and inverse Compton scattering. Such a background is given in chapter 4 and 5. Chapter 8 is dedicated to the recent results in this field and also to a brief look to the near future.

Chapter 2

Radio astronomy

Radio astronomy is a sub-field of astronomy that studies celestial objects at radio frequencies.

Radio waves have frequencies from 300 GHz to as low as 3 kHz, and corresponding wavelengths ranging from 1 millimeter to 100 kilometers. As we can see on figure 2.1, the Earth's atmosphere is very well transparent to radio waves. What makes radio astronomy special is that we can observe also during cloudy day and night. Radio waves are unaffected by dust.

2.1 History of radio astronomy

Compared to the optical astronomy which has history longer than two thousands years, radio astronomy is virtually an infant.

The initial detection of radio waves from an astronomical object was made in the 1930s. Interestingly enough it wasn't performed by an astronomer and on purpose. Karl Jansky, physicist working for Bell Laboratories, was trying to determine the origin of a source of noise that was showing up in long distance radio communications.

He built a big rotating antenna, given the name of *jansky's merry-go-round*. The antenna was designed to receive radio waves at a frequency of 20.5 MHz and with its rotation ability it was able to locate the direction of any radio signal.

After several month of measuring and careful studying of measured data he concluded that noises arose from three different sources. First two originated from nearby and distant thunderstorms. However, the third faint source was somehow different. The location of maximum intensity rose and fell once a day, leading Jansky to suspect that he was detecting radio radiation from the Sun.

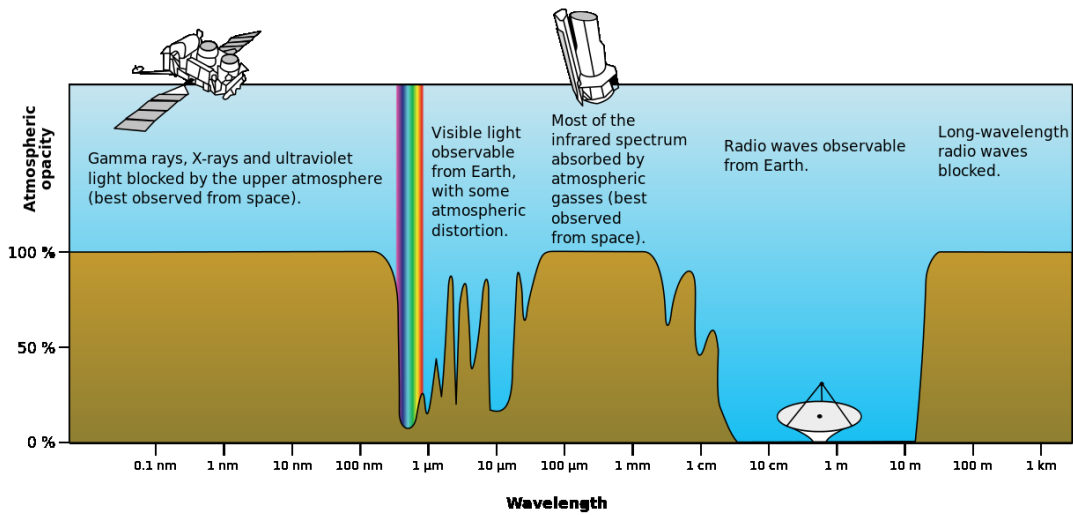


Figure 2.1: Earth's atmospheric opacity to various wavelengths of electromagnetic radiation, including radio waves.[34]

But he kept exploring this mystery.

After another few months of following the signal the brightest point moved away from the position of the Sun. Jansky also determined that the signal repeated on a cycle of 23 hours and 56 minutes, which is the period of the Earth's rotation relative to the stars, so called *sidereal day*. This period is shorter than the period of the Earth's rotation relative to the Sun, *solar day* (24 hours). That was crucial prove that the source is not only extraterrestrial but also originated beyond our Solar System.

By comparing his observations with optical astronomical maps, Jansky concluded that the radiation was coming from the Milky Way and was strongest in the direction of the center of the galaxy, in the constellation of Sagittarius. This was the dawn of radio astronomy.

Jansky's discovery motivated Grote Reber, a radio operator and engineer, to apply for a job with Karl Jansky to further investigate radio waves. Unfortunately Bell Laboratories were not hiring at that time because of the Great Depression. But Reber was determined to answer his questions, even if it meant he had to do it all from his backyard... which eventually he did.

In the summer of 1937, Reber decided to build his own radio telescope in his back yard in Wheaton. Reber's radio telescope was considerably more advanced than Jansky's, consisting of a parabolic metal mirror 9 meters in diameter fo-

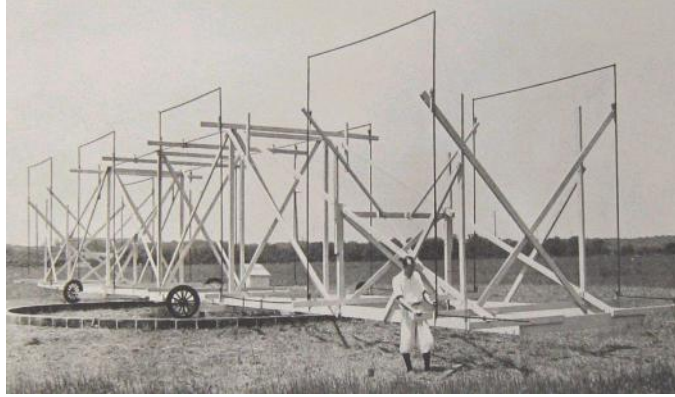


Figure 2.2: Jansky's turnable antennas, [29].

cusing to a radio receiver 8 meters above the mirror. The entire assembly was mounted on a tilting stand allowing it to be pointed in various directions.

His data, published as contour maps showing the brightness of the sky in radio wavelengths, revealed the existence of radio sources such as Cygnus A and Cassiopeia A for the first time.

Since the days of these first pioneers radio astronomy has developed to one of the leading field of astronomy with myriads of fascinating discoveries.

2.2 Radio observation

Radio telescopes most often measure the (spectral) *flux density* of a source. The flux density is the power P received within a certain frequency band $d\nu$, via a certain effective collecting area A with efficiency η :

$$S = 2 \frac{P}{\eta A d\nu}. \quad (2.1)$$

The unit of flux density is $\text{Wm}^{-2}\text{Hz}^{-1}$. The factor of 2 above is because the measurement of power is traditionally only made via one polarisation channel, and it is assumed that the other hand will contribute the same amount of power (in case of unpolarized radiation).

The signals radio astronomers are dealing with are really rather weak. This fact was very nicely demonstrated by Jocelyn Bell Burnell, Northern Irish astrophysicist who, as a postgraduate student, discovered the first radio pulsars



Figure 2.3: Grote Reber in front of his radio telescope, [30].

advised by her thesis supervisor Antony Hewish.

In 1997 when she was giving talk about this discovery she asked everybody to pick up small piece of paper from under the seat where she hid it beforehand. On the paper there was this message: *"In picking up this piece of paper you have used a million times more energy than the radio telescopes receive from all the known pulsars in a year"*. [31]

Even the flux density of one of the strongest radio sources on the the sky Cyg A is around $10^{-22} \text{ Wm}^{-2}\text{Hz}^{-1}$. Instead of using such a small numbers radio astronomers adopted a non-SI unit of spectral flux density, *jansky* (symbol Jy). It is defined as following:

$$1 \text{ Jy} = 10^{-26} \text{ Wm}^{-2}\text{Hz}^{-1}. \quad (2.2)$$

Using this unit Cyg A has the flux density of around 10 000 Jy at 150 MHz.

2.3 Brightness temperature

The electromagnetic radiation emitted by a black body is described by the *Planck function*:

$$B_\nu(T) = \frac{2h\nu^3/c^2}{e^{h\nu/kT} - 1}. \quad (2.3)$$

For $h\nu/kT \ll 1$, using following relation:

$$e^{\frac{h\nu}{kT}} \sim 1 + \frac{h\nu}{kT},$$

we get the *Raleigh-Jeans law*:

$$B_\nu(T) = \frac{2kT\nu^2}{c^2}. \quad (2.4)$$

The Raleigh-Jeans law holds all the way through the radio regime for any reasonable temperature. Even though radiation mechanisms in radio astronomy are often non-thermal, radio astronomers are talking about the *brightness temperature* of a source. That is the equivalent or effective temperature that a blackbody would need to have in order to be that bright:

$$T_B = \frac{B_\nu(T)c^2}{2k\nu^2}. \quad (2.5)$$

One must be really careful when interpreting this quantity. For example, Cyg-A has $T_B \sim 10^7$ K ([11]). It is not a physical temperature but a measure of the energy density of the electrons and magnetic fields that generate radio emission in this case via non-thermal synchrotron emission.

We can get two cases when measuring the flux density (see figure 2.5). First one is when the telescope observes a radio source that is smaller or the same size as the telescope beam. The second one is when the telescope observes a radio source that is larger than the telescope beam. Clearly, in the later case the measured flux density is smaller than the total flux density of the source.

This leads to the fact that a larger telescope (with narrower beam as we will see later) will measure a smaller flux density of this radio source. That is why in radio maps or images surface brightness is often given in a unit *Jy per beam*. In fact, this is nothing else than specific intensity.

Now we can go back to the flux density S . The flux density is specific intensity integrated over solid angle. In our case specific intensity is equal to the Planck function.

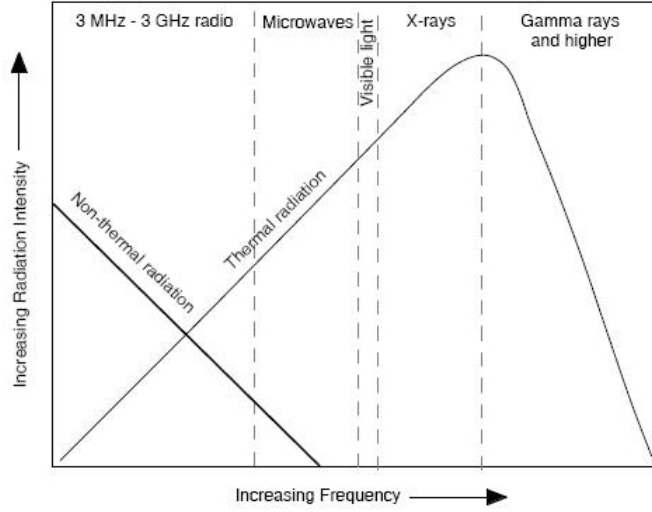


Figure 2.4: The intensity (energy) of thermal radiation increases with frequency whereas the intensity of non-thermal radiation usually decreases with frequency.[38].

$$S_\nu = \int I(\nu) d\Omega = \int 2kT_B \nu^2 / c^2 d\Omega = 2k\nu^2 / c^2 \int T_B d\Omega. \quad (2.6)$$

Hence the flux density is just the brightness temperature integrated over the source.

2.4 Radio telescopes

Radio photons are too weak to do much so we cannot usually detect individual photons (unlike optical or high-energy observations). Instead we must think classically in terms of measuring the source electric field.

The easiest way to do it is by using dipole antenna. Electric field of incoming radiation induces currents in the antenna and we can subsequently measure the voltage in a resistor. Dipole length must be kept short, length $< \lambda$ (the wavelength of received radio radiation). It needs to be mentioned that any antenna is only sensitive to one polarisation because current is only induced by field that is parallel to dipole axis.

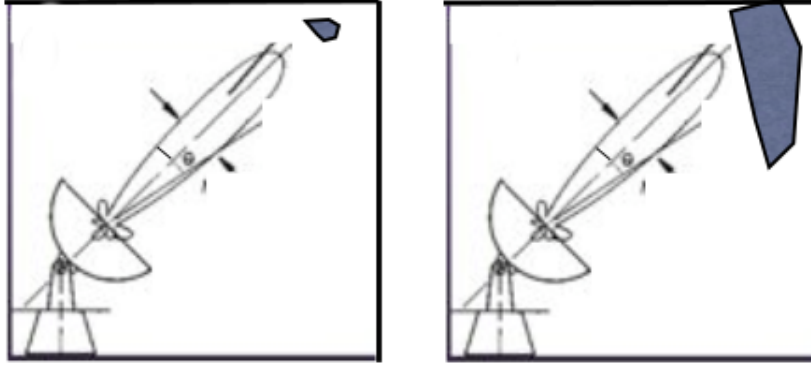


Figure 2.5: Observing resolved sources with radio telescopes can lead to two cases, [39].

In a parabolic *dish* telescopes (figure 2.6) incoming electromagnetic wave's electric field oscillations induce voltage oscillations at the antenna focus, in a device called a *feed*. A feed collect the incoming radio waves, convert them to electric currents and transmit them to the *receiver*. A radio receiver is an electronic device that receives radio waves and converts the information carried by them to a usable form.

Important characteristic of an antenna is *the directivity* or in another words *max gain*, denoted as G . It is a figure of merit for an antenna. It measures the power density the antenna radiates in the direction of its strongest emission, versus the power density radiated by an ideal isotropic radiator (which emits uniformly in all directions) radiating the same total power (see figure 2.7). It is often given in dB, *decibels above an isotropic radiator*.

The simplest antenna is the half-wave dipole with length $\lambda/2$. For such a antenna $G \sim 1,6\text{dB}$. That is not much better than isotropic radiator. The gain can be improved by combining together the output of several dipoles arranged in an array.

It can be shown that the effective area of a lossless isotropic antenna, which by definition has unity gain, is:

$$A = \frac{\lambda^2}{4\pi}, \quad (2.7)$$

where λ is the wavelength of radiowaves. So the gain of any antenna is propor-



Figure 2.6: Lovell parabolic telescope, [41]

tional to its effective area:

$$G = \frac{4\pi}{\lambda^2} A. \quad (2.8)$$

This means that antennas with large effective area are high gain antennas, which have small angular beam widths. Most of their power is radiated in a narrow beam in one direction, and little in other directions. As receiving antennas, they are most sensitive to radio waves coming from one direction, and are much less sensitive to waves coming from other directions.

Another important quantity is the *antenna temperature*. Antenna temperature T_A is a parameter that describes how much noise an antenna produces in a given environment. This temperature is not the physical temperature of the antenna. The definition says that antenna temperature is the temperature that a resistor would have if it was to generate the same power density at frequency ν as that observed from the antenna port,[3]. Therefore, an antenna does not have an intrinsic "antenna temperature" associated with it; rather the temperature depends on its gain pattern and the thermal environment that it is placed in. The noise power received from an antenna can be then expressed as:

$$P = kT_A d\nu, \quad (2.9)$$

where k is The Boltzmann constant. The receiver also has associated temperature T_R and the total system temperature (antenna plus receiver) has a combined

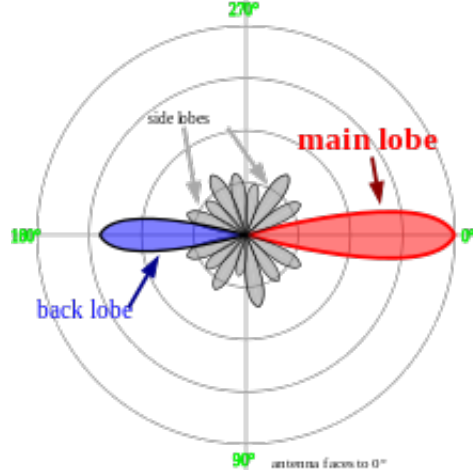


Figure 2.7: Diagram showing directivity, [40].

temperature given by:

$$T_{\text{SYS}} = T_{\text{A}} + T_{\text{R}} \quad (2.10)$$

The total noise power of the system is then:

$$P = kT_{\text{SYS}}d\nu. \quad (2.11)$$

2.5 The noise

What makes the biggest different between radio astronomy and astronomy in shorter wavelengths (whether it is infrared astronomy, visible astronomy or UV/X-ray astronomy) is the fact mentioned at the beginning of the previous section; radio photons are simply too weak to do much. So it is inevitable to amplify the incoming signal even before its power is measure whereas in higher frequencies the energy of incoming stream of photons is counted directly.

No matter at which frequency the astronomer is measuring, he or she always has to deal with extraneous noise signals that corrupts the observations. This is especially painful in radio band since the cosmic radio signal is usually much more weaker than the noise (by several orders of magnitudes). That is why it is absolutely essential to be able to specify the total system temperature (Eq.2.10) and to try to minimize it as much as possible.

The sources of noises are several and all of them contribute to the total system temperature. As was already mentioned, one of them is the antenna system

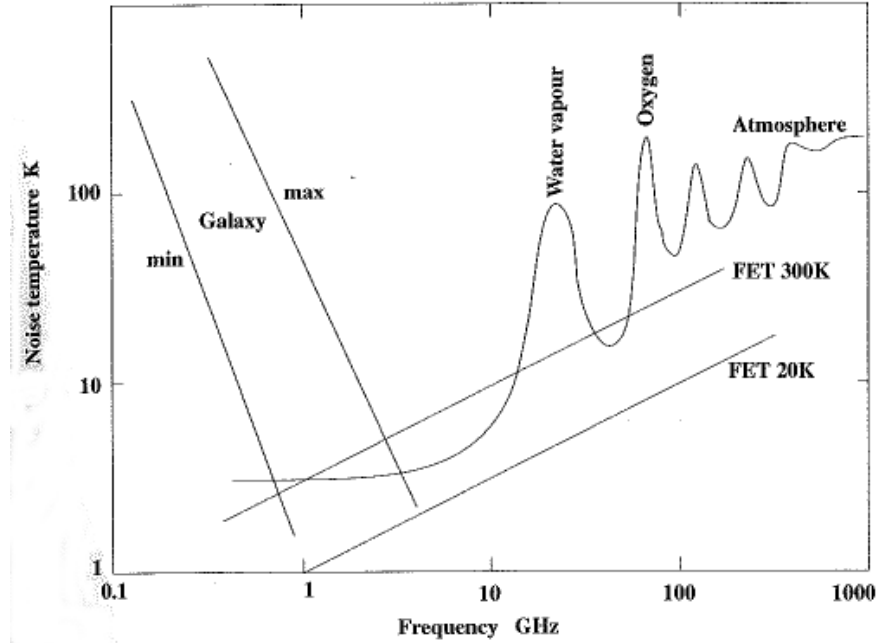


Figure 2.8: Antenna and receiver noise temperatures (FET means Field-Effect Transistors and the values presented on the graph are the current state of the art) compared to the noise temperature from our atmosphere and galactic background noise, [3].

itself, the main exterior source of noise is our atmosphere. The importances of individual sources are different in different frequencies (illustrated on figure 2.8).

The block diagram of a radio telescope is shown on figure 2.9. More specifically it is a diagram showing a radio telescope with so called *heterodyne receiver* because it incorporate a *frequency converter* (often called a mixer) that shifts the initial frequency band (but apart of that preserves the signal). The system has to be calibrated to the noise. How this is done is described in [3].

2.6 Radio interferometry

This section is based on National Radio Astronomy observatory (NRAO) online course [42].

The angular resolution of any kind of telescope (no matter in which part of

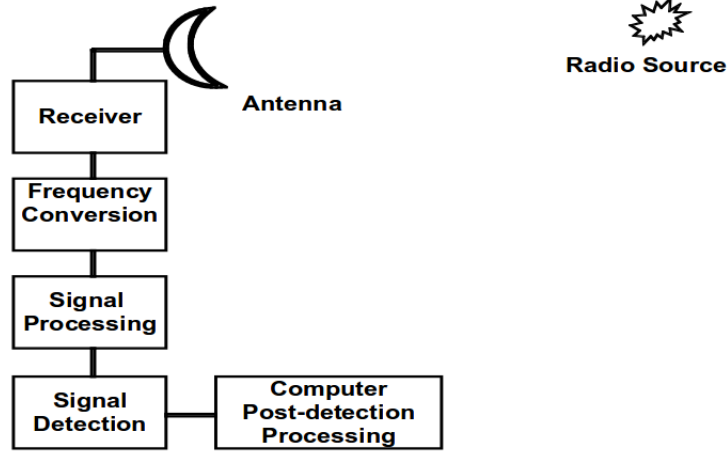


Figure 2.9: Radio Telescope block diagram, [39].

electromagnetic spectrum it is observing) is given by formule:

$$\Theta = \frac{1.22\lambda}{D}, \quad (2.12)$$

where D is the diameter of the aperture.

Let's now compare the resolution of human eye and compare it with the resolution of Effelsberg 100-m diameter radio telescope:

$$\Theta_{\text{eye}} \simeq \frac{1.2 \times 550 \text{ nm}}{5 \text{ mm}} = 28 \text{ arcsec}. \quad (2.13)$$

For Effelsberg telescope at 3 cm wavelength (10 GHz):

$$\Theta_{\text{Effelsberg}} \simeq \frac{1.2 \times 3 \text{ cm}}{100 \text{ m}} = 70 \text{ arcsec}. \quad (2.14)$$

So a human eye has better angular resolution than one of the biggest radio telescope in the world!

Arc-minute resolution is often not good enough to resolve the detailed structure of many astrophysical objects e.g. distant galaxies, quasars etc.

But if we engage more telescopes the angular resolution will be given by formula:

$$\Theta = \frac{1.22\lambda}{B}, \quad (2.15)$$

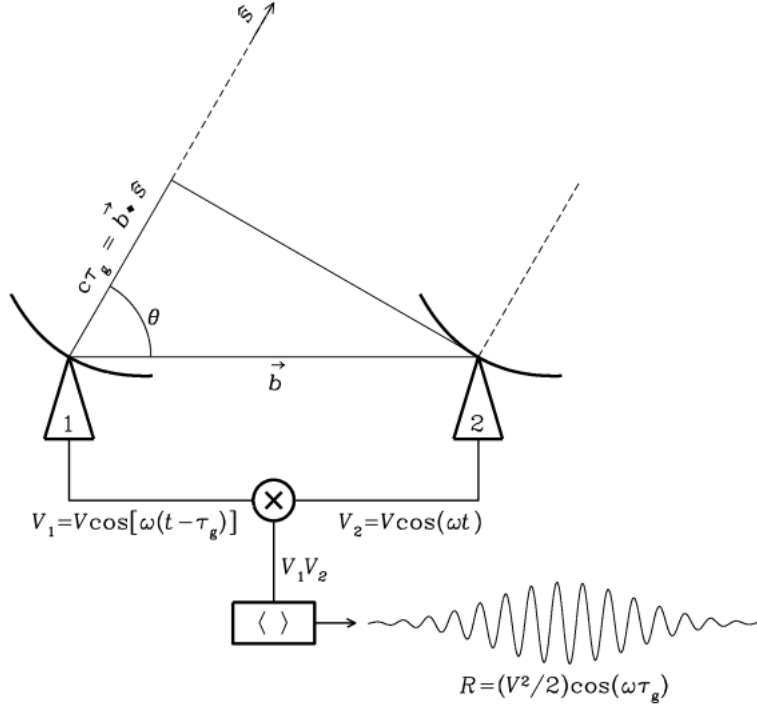


Figure 2.10: The block diagram showing the components of two-element interferometer, [42].

where B is a baseline i.e. telescope separation.

The basic interferometer is a pair of identical radio telescopes separated by a baseline vector of length b whose voltage outputs are correlated, that means multiplied and averaged. The set up is shown on figure 2.10.

Both dishes are pointing to the direction specified by \hat{s} (hat means it is a unit vector). Plane waves from a distant point source in this direction must travel an extra distance $\vec{b} \cdot \hat{s} = b \cos \theta$, so the output of antenna 1 is the same as that of antenna 2, but it lags by the *geometric delay*: $\tau_g = \vec{b} \cdot \hat{s} / c$.

We focus on *quasi-monochromatic* interferometer. That is one that responds only to radiation in a very narrow band centered on frequency $\nu = \omega / (2\pi)$. The output voltage of antennas 1 and 2 can be then written as:

$$V_1 = V \cos [\omega(t - \tau_g)], \quad V_2 = V \cos(\omega t), \quad (2.16)$$

where t is time.

The *correlator* first multiplies these two voltages to yield the product:

$$V_1 V_2 = V^2 \cos(\omega t) \cos[\omega(t - \tau_g)] = \left(\frac{V^2}{2} [\cos(2\omega t - \omega\tau_g) + \cos(\omega\tau_g)] \right) \quad (2.17)$$

and then take a time average long enough [$\delta t \gg (2\omega)^{-1}$] to remove the high-frequency term $\cos(2\omega t - \omega\tau_g)$ from the final output R :

$$R = \langle V_1 V_2 \rangle = \frac{V^2}{2} \cos(\omega\tau_g). \quad (2.18)$$

The amplitude V_1, V_2 are proportional to the electric field produced by the source multiplied by the voltage gains of antennas. Thus the output amplitude $V^2/2$ is proportional to the point-source flux density S multiplied by $(A_1 A_2)^{1/2}$, where A_1, A_2 are the effective areas of the two antennas.

The big advantage is that uncorrelated noise from the receivers and the atmosphere does not appear in the correlator output, so fluctuations in receiver gain or atmospheric emission are much less significant than for observation with a single antenna.

2.7 Radio sky

The sky in radio wavelengths looks quite different from the visible sky. Most bright stars are undetectable at radio frequencies and many strong radio sources are optically faint or invisible.

Remarkable difference is also in the distances to the point sources in visible sky and radio sky. Unlike the nearby stars visible to the human eye, almost none of the *radio stars* (unresolved radio sources) are actually stars. Most of them are extremely luminous radio galaxies or quasars. Their average distance is over 5 billions light years!

Radio emission has origin in various physical mechanism. Three different processes generate continuum radio radiation. The Moon and planets emit thermal radiation (Jupiter is strong non-thermal source as well thanks to the electrons in it's magnetic field). Very important source of radio thermal radiation is cosmic microwave background.

The second process is bremsstrahlung (free-free emission). It is a major part of the radio spectrum observed from HII regions.

The third process is synchrotron emission. It is associated with a wide variety of radio-energy emitters, including supernova remnants such as the Crab Nebula



Figure 2.11: This composite picture shows the radio sky at 4.85 GHz above an optical photograph. The brightest irregularly shaped sources are clouds of hydrogen ionized by luminous young stars. source: NRAO 300ft Survey [32].

and Cassiopeia A; and pulsars. The synchrotron mechanism is also in effect in two other major radio sources, radio galaxies and certain quasars. The synchrotron radiation is discussed in chapter 4.

The example of line radiation is the 21-cm line spectral line of neutral hydrogen HI. The brightness of the 21 cm hyperfine line at 14 204 MHz is proportional to the column density of HI along the line of sight and is nearly independent of the gas temperature. It is not affected by dust absorption, so we can see the HI throughout our Galaxy and nearby external galaxies.

Chapter 3

Active galactic nuclei

Active galaxies are highly luminous galaxies with non-thermal spectrum often with strong emission lines that do not look like the sum of many stellar spectra (see figure 3.1). They are also highly variable. Often they are called *Active Galactic Nuclei* (AGN) because their nuclei are their main feature.

3.1 AGN types

Carl Seyfert discovered the first class of AGN, that are now named after him [15]. The nuclei of *Seyfert galaxies* has very high surface brightnesses and display strong, high-ionisation emission lines. But their host galaxies are still clearly detectable.

Type 1 Seyfert galaxies have both narrow and broadened optical spectral emission lines. *Seyfert type 2 galaxies* have narrow emission lines only (but still wider than emission lines in normal galaxies).

Quasars or quasi-stellar radio sources are the most luminous AGN typically 1 000 times the luminosity of our Galaxy. The spectra of quasars are similar to Seyferts except that stellar absorption features are weak or absent, and the narrow emission lines are weaker relative to broad lines as seen in Seyferts. Another difference from Seyfert galaxies is that their host galaxies are not detectable. Most of them are visible at redshift $z \geq 2$.

BL Lac objects are named after BL Lacertae, the class prototype. In contrast to other types of active galactic nuclei, BL Lacs are characterized by rapid and large-amplitude flux variability and significant optical polarization.

Radio galaxies, as their name implies, are strong emitters of radio emission. For the most part, radio galaxies are giant ellipticals with absolute visual mag-

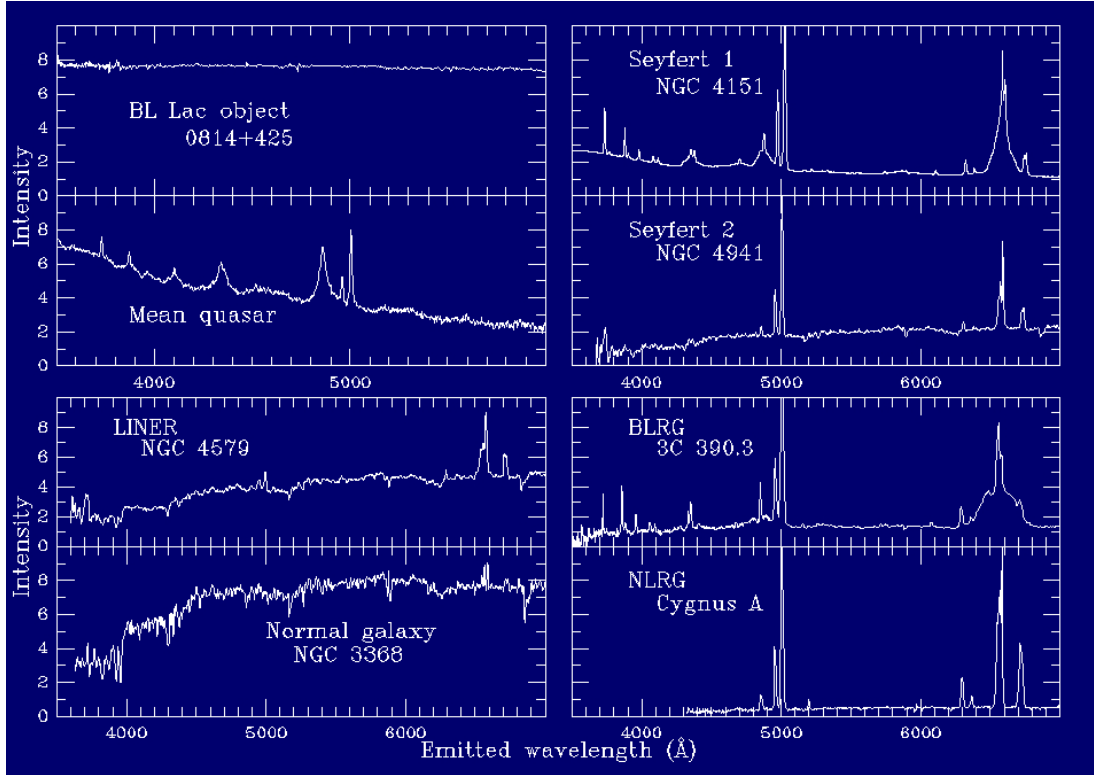


Figure 3.1: Examples of AGN spectra, compared to the spectrum of normal galaxy (right bottom spectrum). Their main difference is the presence of strong emission lines in AGN spectra (except for BL Lac objects), author: Bill Keel [35].

nitide about -21. They often exhibit jet structure from a compact nucleus and also two lobes of radio frequency emission that are often approximately aligned with the jets observed in the visible spectrum and that may extend for millions of light years.

The radio emission is non-thermal, due to fast moving electrons that spiral in magnetic fields, producing synchrotron emission (chapter 4).

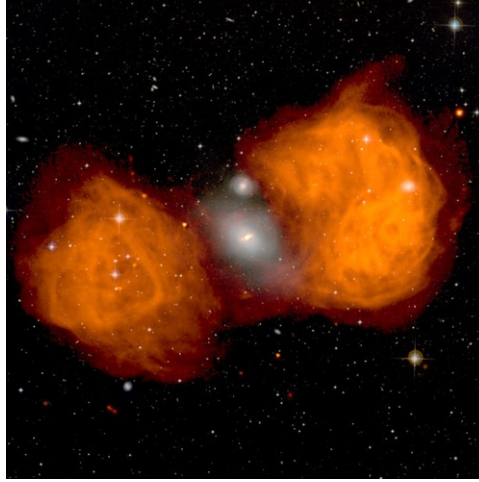


Figure 3.2: Fornax A (also known as NGC 1316) is an example of radio galaxy. This image shows the radio emission (shown in orange, imaged using the Very Large Array in New Mexico) superimposed on an optical image (STScI/POSS-II), source:[36]

3.2 Unification of AGN species

Even if it sounds surprising, it is now believed that all the above mentioned objects can be unified in one model.

The currently favoured unified model of all AGN species propose that the apparent differences between different types of AGNs are the result of different orientation of single type physical object to the observer [13]. The asymmetric nature of the object gives rise to the diversity of observed properties (see the well-known illustration of this model on figure 3.4).

In this model, an active galactic nucleus has a massive black hole with mass at least $10^6 M_{\odot}$ in its center. The energy of the AGN comes from gravitational potential energy of the material surrounding the black hole (this material consists of inter stellar material and also of disrupted stars). In the process of falling into the black hole, a considerable fraction of the rest-mass energy is released (about 10 % , making it the most efficient known way of using mass to get energy, compare it to efficiency of nuclear fusion - 0.4 %).

Around the thin inner accretion disk, there is a thicker torus of cooler accreting material. This torus is opaque, making it impossible to see the central feature through it. Another important part of this model is the pair of jets ejected from

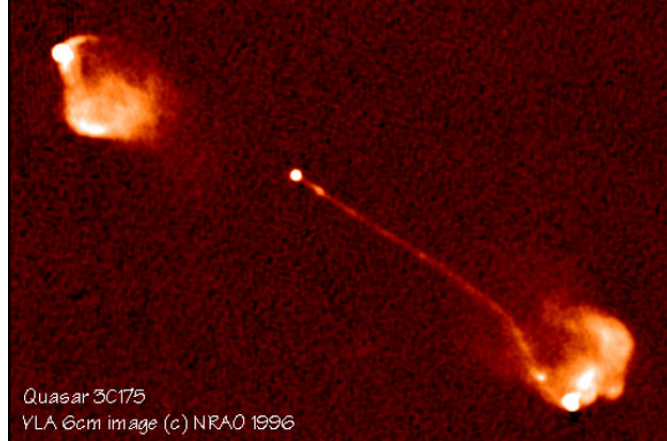


Figure 3.3: This image shows the radio emission from relativistic streams of high energy particles generated by the FR II radio galaxy 3C175. This is a classic double-lobed radio source. The image was recorded by the Very Large Array, source:[37].

the center along the polar directions. These flows of energetic particles may travel very large distances in comparison with the size of the obscuring torus forming the double structures as the one on figure 3.3.

3.3 Super massive black holes

Various techniques inferred presence of an supermassive black hole (SMBH) with mass ranges from $\sim 10^6$ to $10^{10} M_{\odot}$ at centre of nearly every nearby galaxy (The Milky Way included). The main and unambiguous evidences are based on star and gas dynamics. For instance in the Milky Way, M31 and M32 the mean square velocities of the stars or gas rises as $\sim 1/r$ near the center, indicating a central point mass [5], [6]. Important question now is: is an SMBH at the centre of an galaxy somehow bounded with the evolution of galaxy?

Big step towards understanding this question was made in 1999. The $M - \sigma$ relation was first presented then [7], [8]. It is an empirical correlation between the stellar velocity dispersion σ of a galaxy bulge (the central group of stars in spiral galaxies) and the mass M of the supermassive black hole at its center. As can be seen on figure 3.5 there is undeniable relation.

According to recent study [9], based on a complete sample of published black

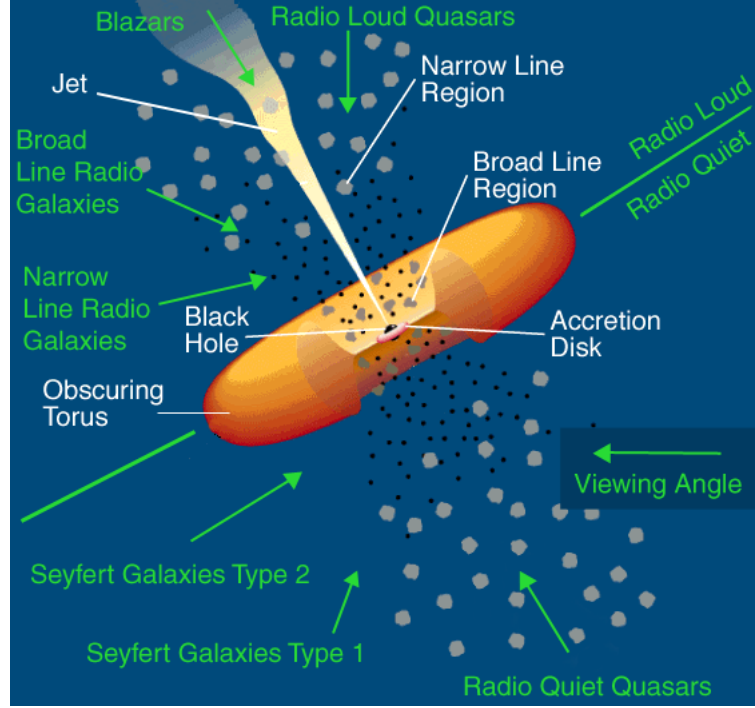


Figure 3.4: Unified model for AGNs, image credit: NASA.

hole masses in nearby galaxies, the relation is:

$$\frac{M}{10^8 M_{\odot}} \approx 1.8 \left(\frac{\sigma}{200 \text{ km s}^{-1}} \right)^{5.1}. \quad (3.1)$$

Could it be explained simply by the influence of the black hole on the stellar kinematics of the nucleus? No, since most of velocity dispersion measurements were carried out using aperture much larger than the expected radius of gravitational influence of the black hole. But the black hole mass is tightly coupled to velocity dispersion of the host galaxy over 3 magnitude. It suggests a causal connection between the formation and evolution of the black hole and the bulge.

This means that there must be some source of feedback between the growth of SMBHs and the growth of galaxy bulges, although the exact mechanism remains uncertain.

Possible explanation is featuring the AGN. When there is enough material supply, SMBH accretes and AGN is formed. Radiation, winds and jets from the active nucleus of a massive galaxy can interact with its interstellar medium

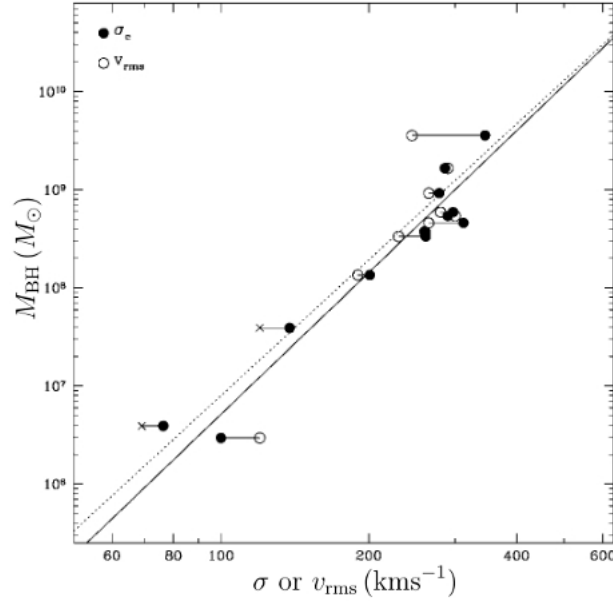


Figure 3.5: Black hole mass vs. the central velocity dispersion of the hot elliptical galaxy or bulge.[7].

(sometimes even with intergalactic medium) leading to ejection or heating of the gas. This can terminate star formation and stifle accretion onto the black hole. But as it was said before, how exactly does the energy and momentum transfer proceed remains mystery with. First glimpses were made by observing cold HI outflows in galaxies. ([12]).

Nevertheless, what is absolutely clear is that a SMBH is critical component of galaxies and that one way of trying to understand the role of the central black holes is through AGNs. So trying to constrain the time scales of AGN duty cycles might influence the understanding of formation and evolutions of galaxies.

Chapter 4

Synchrotron emission

Charged particles accelerated by a magnetic field will radiate since they move in a helical path (they are being accelerated), and therefore radiate electromagnetic radiation.

For nonrelativistic velocities the complete nature of the radiation is rather simple and is called *cyclotron radiation*. Non-relativistic electron orbits with a velocity-independent angular frequency, the *gyro-frequency*:

$$\omega_G = \frac{eB}{m_e c}. \quad (4.1)$$

However, for relativistic particles the frequency spectrum is much more complex since the energy emitted does not depend only on the magnetic field but also on the energy of the particles themselves. This radiation is known as *synchrotron radiation*.



Figure 4.1: Charged particle in magnetic field.

Spectral properties of synchrotron emission are tightly bounded with the effect of *beaming*.

4.1 The beaming effect

The beaming effect is the process by which relativistic effects modify the apparent luminosity of emitting matter that is moving at speeds close to the speed of light. Personally, I like the formulation that says that *beaming is the geometric expression of the relativity of simultaneity*.

To understand the beaming effect, let me start with another effect called aberration.

Aberration is the change in an object's apparent direction caused by the relative transverse motion of the observer.

The definition says nothing about relativistic speeds. And indeed, we can experience aberration in our everyday, surely non-relativistic, life.

Consider a person standing in the rain on a day when there is no wind. If the person is standing still, then the rain drops will follow a path that is straight down to the ground. However if the person is riding a car, the rain will appear to be approaching at an angle. As he travels faster, the angle of inclination increases. This apparent change in the direction of the incoming raindrops is the aberration.

The amount of aberration depends on the speed of the emitted object or wave relative to the observer. In the example above this would be the speed of a car compared to the speed of the falling rain.

Now we can proceed to the relativistic case and that means we will need Lorentz transformation. For two inertial frames with a relative velocity v along the x axis, the relations between x y z t and x' y' z' t' in the moving frame are (every quantity in rest frame is denoted with prime symbol, e.g. x'):

$$\begin{aligned}x' &= \gamma(x - vt) \\y' &= y \\z' &= z \\t' &= \gamma\left(t - \frac{v}{c^2}x\right),\end{aligned}$$

where

$$\gamma = \left(1 - \frac{v^2}{c^2}\right)^{-1/2}.$$

With the Lorentz transformations for differentials:

$$\begin{aligned}dx &= \gamma(dx' + vdt') \\dy &= dy' \\dz &= dz' \\dt &= \gamma(dt' + \frac{v}{c^2}dx'),\end{aligned}$$

we get the transformation of velocities as following:

$$\begin{aligned}u_x &= \frac{dx}{dt} = \frac{u'_x + v}{1 + vu'_x/c^2} \\u_y &= \frac{u'_y}{1 + vu'_x/c^2} \\u_z &= \frac{u'_z}{1 + vu'_x/c^2}.\end{aligned}$$

We can generalize these equations to an arbitrary velocity v . The velocity u can be then stated in terms of the components perpendicular to and parallel to v :

$$\begin{aligned}u_{\parallel} &= \frac{u'_{\parallel} + v}{(1 + vu'_{\parallel}/c^2)}, \\u_{\perp} &= \frac{u'_{\perp}}{\gamma((1 + vu'_{\parallel}/c^2))}.\end{aligned}$$

The direction of the velocities in the two frames are related by the *aberration formula*:

$$\text{tg}\theta = \frac{u_{\perp}}{u_{\parallel}} = \frac{u'\sin\theta'}{\gamma(u'\cos\theta' + v)}$$

Lets see what happens when the u' is the velocity of light in vacuum c . Then:

$$\begin{aligned}\text{tg}\theta &= \frac{\sin\theta'}{\gamma(\cos\theta' + v/c)}, \\ \cos\theta &= \frac{\cos\theta' + v/c}{1 + (v/c)\cos\theta'}.\end{aligned}$$

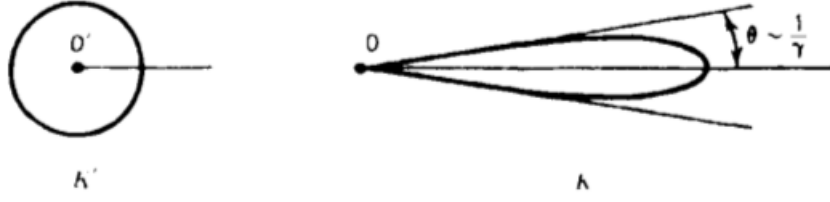


Figure 4.2: Relativistic beaming of radiation emitted isotropically in the rest frame K' . In the laboratory frame K highly relativistic electrons radiate in a narrow beam with width of order $1/\gamma$ in the direction of motion. [1]

Useful and instructive case is the one with $\theta' = \pi/2$ that is, a photon is emitted at right angles to v in K' . Then we get:

$$\tan \theta = \frac{c}{\gamma v}$$

$$\sin \theta = \frac{1}{\gamma}$$

For $\gamma \gg 1$ (means the speed of K' is highly relativistic):

$$\theta \sim \frac{1}{\gamma}.$$

If photons are emitted isotropically in K' , then half will have $\Theta' < \pi/2$ and $\Theta' > \pi/2$. Then in frame K photons are concentrated in the forward direction, with half of them lying within a cone of half-angle $1/\gamma$. Very few photons will be emitted having $\Theta \gg 1/\gamma$.

4.2 Synchrotron power from a single electron

In the electron rest frame electron emits cyclotron power. But in the laboratory frame where this electron is moving relativistically, the radiation pattern becomes highly beamed as we can see on the figure 3.2 with very little power radiated in the backward direction and with the much narrower beam. As the result of this beam being much narrower an observer observing synchrotron emission receives photons for a shorter period of time. That is what makes it different from cyclotron radiation. Cyclotron radiation comes with gyro-frequency ω_G (3.1) while

synchrotron emission arrives at a variety of frequencies up to a characteristic cut-off frequency:

$$\omega_{\text{cutoff}} = \frac{3}{2}\gamma^2\omega_G\sin\Theta, \quad (4.2)$$

where Θ is the angle electron's velocity makes relative to the direction of the magnetic field. This angle is called *pitch angle*. Because of the lorentz factor, which can be of order $10 \sim 100$, synchrotron emission is much harder than cyclotron emission.

Larmor formula gives us the total power radiated by a non relativistic point charge q as it accelerates or decelerates (in cgs units):

$$P = \frac{2}{3} \frac{q^2 a^2}{c^2}. \quad (4.3)$$

It can be shown that the total power is lorentz invariant which means that under lorentz transformations power is unchanged. Everybody can agree what the power radiated is.

So in order to get the synchrotron emission in the laboratory frame (from Larmor formula) all we have to do is calculate the power P' radiated in the electron's frame. Which means we have to figure out what the acceleration in the electron rest frame a' is. For this we will use the expression for lorentz force:

$$\vec{F}' = m_e a' = e \left(\vec{E}' + \vec{v} \times \vec{B}' \right) \quad (4.4)$$

For general case the EM field transforms under lorentz transformation as following:

in the direction parallel to the velocity vector:

$$E'_{\parallel} = E_{\parallel}, \quad B'_{\parallel} = B_{\parallel}, \quad (4.5)$$

and in the perpendicular direction:

$$\vec{E}'_{\perp} = \gamma(\vec{E}_{\perp} + \frac{\vec{v}}{c} \times \vec{B}), \quad \vec{B}'_{\perp} = \gamma(\vec{B}_{\perp} - \frac{\vec{v}}{c} \times \vec{E}). \quad (4.6)$$

In the laboratory frame we do not *see* any electric field \vec{E} and also we are not interested in any B' fields in the electron's frame since the electron is not moving (in the electron rest frame) so the B' field cannot be responsible for acceleration.

In the end the electric field in the electron rest frame is given by:

$$\vec{E}'_{\parallel} = 0, \quad (4.7)$$

$$\vec{E}'_{\perp} = \gamma \frac{\vec{v}}{c} \times \vec{B} = \frac{Bv}{c} \sin \Theta. \quad (4.8)$$

The acceleration in electron's rest frame is then:

$$a' = \frac{eE'}{m_e} = \frac{eB}{m_e c} \gamma v \sin \Theta. \quad (4.9)$$

and the power radiated in electron's rest frame:

$$P' = \frac{2}{3} \frac{e^4 B^2 \gamma^2 v^2}{m_e^2 c^5} \sin^2 \Theta. \quad (4.10)$$

In the lab frame where the electron is travelling with the velocity so close to speed of light that we can use c instead of v , we get (using $P = P'$):

$$P = \frac{2}{3} \frac{e^4 B^2}{m_e^2 c^3} \gamma^2 \sin^2 \Theta. \quad (4.11)$$

if we use the expression for *Thomson cross-section*:

$$\sigma_T = \frac{8\pi}{3} \left(\frac{e^2}{m_e c^2} \right)^2 \quad (4.12)$$

we can rewrite the power as:

$$P = 2\sigma_T c \frac{B^2}{8\pi} \gamma^2 \sin^2 \Theta. \quad (4.13)$$

The quantity $B^2/8\pi$ is the energy density of magnetic field U_B . So the another expression for synchrotron power from single electron is:

$$P = 2\sigma_T c U_B \gamma^2 \sin^2 \Theta. \quad (4.14)$$

For isotropic distribution of electrons we can use the pitch angle averaged term: $\langle \sin^2 \Theta \rangle = 2/3$. In such a case Eq.4.14 becomes:

$$P = \frac{4}{3} \sigma_T c U_B \gamma^2. \quad (4.15)$$

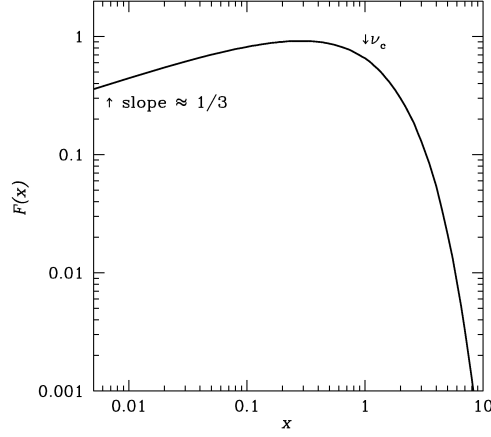


Figure 4.3: The spectrum of synchrotron emission from single electron.

4.3 The spectral shape of synchrotron radiation

The spectrum of synchrotron emission from single electron looks like the one on the figure 4.3. There is a peak defined by cut-off frequency (3.2). At lower frequencies the spectrum has $\nu^{1/3}$ dependence. We can also say that the *spectral index* α is $-1/3$ (I am using the sign convention in which the spectral index is given by $S \propto \nu^{-\alpha}$). Above the cut-off frequency there is a rapid exponential dampening with $P_\nu \sim \nu^{1/2}e^{-\nu}$.

Normally we do not have just one electron as a source but there is an ensemble of electrons. And since the cut-off frequency (3.2) depends on γ we need to make some assumptions. First we assume that our ensemble has an isotropic pitch-angle distribution. The energy distribution of the radiating electrons in many synchrotron sources is in the form of a power law, so we assume it is also our case:

$$\frac{dN}{dE} = CE^{-p}, \quad (4.16)$$

or we can also express it in the terms of γ as:

$$\frac{dN}{d\gamma} = C\gamma^{-p}, \quad (4.17)$$

where p is the spectral index and C is constant.

The total power radiated per unit volume per unit frequency by such a distribution is given by the integral of $N(\gamma)d\gamma$ times the spectrum of single electron

(4.11) over all energies or γ . Thus, we have:

$$P_{\text{tot}}(\omega) = C \int_{\gamma_1}^{\gamma_2} P(\omega) \gamma^{-p} d\gamma \propto \int_{\gamma_1}^{\gamma_2} F\left(\frac{\omega}{\omega_{\text{cutoff}}}\right) \gamma^{-p} d\gamma. \quad (4.18)$$

If we change the variables of integration to $x \equiv \omega/\omega_{\text{cutoff}}$, taking into account that $\omega_{\text{cutoff}} \propto \gamma^2$, we get:

$$P_{\text{tot}}(\omega) \propto \omega^{-(p-1)/2} \int_{x_1}^{x_2} F(x) x^{(p-3)/2} dx. \quad (4.19)$$

The limits x_1 and x_2 depends on ω . However, if the energy limits are sufficiently wide we can approximate $x_1 \approx 0$, $x_2 \approx \infty$, so that the integral is approximately constant. In that case, we have:

$$P_{\text{tot}} \propto \omega^{-(p-1)/2}. \quad (4.20)$$

The spectral index is then related to the particle energy distribution index p by:

$$s = \frac{p-1}{2}. \quad (4.21)$$

4.4 Self-absorbed synchrotron radiation

For every emission process there is an associated absorption process. For synchrotron emission the associated absorption process is called *synchrotron self-absorption*, in which a photon interacts with a charge in a magnetic field and is absorbed, giving up its energy to the charge. The emitting particles in a source in local thermodynamic equilibrium have a Maxwellian energy distribution, and such a source is called a *thermal source*. In such a case, the source cannot have brightness temperature T_{B} (1.5) greater than the particle temperature T . The emission and self-absorption are balanced.

Astrophysical synchrotron sources are often called *nonthermal* sources because the energy distribution of the relativistic electrons is a power law (3.15) and there is no single electron temperature T . However, self-absorption still occurs, regardless of the energy distribution.

We can associate a *kinetic effective temperature* T_e with electrons of a given energy through the relativistic formula:

$$\gamma m_e c^2 = 3kT_e. \quad (4.22)$$

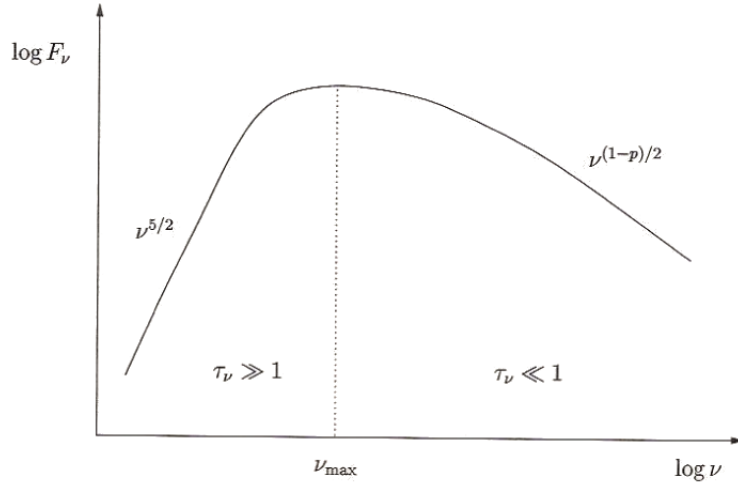


Figure 4.4: The synchrotron spectrum of a source with a power law electron distribution.

We can see that the kinetic effective temperature of the electrons is a function of their energy. Using the fact $\gamma \approx (\omega/\omega_{\text{cutoff}})^{1/2}$:

$$T_e \approx \frac{m_e c^2}{3k} \left(\frac{\omega}{\omega_{\text{cutoff}}} \right)^{1/2}. \quad (4.23)$$

If the radiating source is optically thick ($\tau_\nu \gg 1$), the brightness temperature T_B is equal to T_e . If we want to obtain the flux density in the Rayleigh-Jeans limit(1.4) we use equation 1.6:

$$S_\nu = 2k\nu^2/c^2 \int T_B d\Omega = 2k\nu^2/c^2 \int T_e d\Omega = \frac{2m_e}{3\nu_{\text{cutoff}}^{1/2}} \Omega \nu^{5/2} \propto \frac{\Theta^2 \nu^{5/2}}{B^{1/2}}, \quad (4.24)$$

where Ω is the solid angle subtended by the source and if the angular size of the source is Θ , then $\Omega \approx \Theta^2$.

We have ended up with quite interesting result. The spectrum is a power law with spectral index $-5/2$, independent of the value of p from 3.15. We can also compare this spectral index with the spectral index $s = -2$ for optically thick radiation from a source in full thermodynamics equilibrium.

For optically thin $\tau_\nu \ll 1$ the spectrum of synchrotron emission has the spectral index as derived in 3.20. The final synchrotron spectrum from a power-law distribution of electrons can be seen on figure 3.4.

Synchrotron self-absorption is encountered notably in the compact quasar-like sources known as gigahertz-peaked sources (section 6.2).

Chapter 5

Inverse Compton scattering

Compton scattering is the inelastic scattering of a photon by a charged particle, usually an electron. It results in a decrease in energy of the photon (which may be an X-ray or gamma ray photon).

If, on the other hand, relativistic electron encounters low-energy photon, Compton scattering can transfer energy from the electrons to the photons, boosting them even to gamma-ray energy. So the photon gains and the electron losses energy. This is called *inverse Compton scattering*.

The power produced by inverse Compton scattering (I am not going into the detailed derivation (it can be found in Rybicki Lightman [1])) is for the electrons encountering an isotropic distribution of photons:

$$P = \frac{4}{3} \sigma_{\text{T}} c \frac{v^2}{c^2} U_{\text{rad}} \gamma^2, \quad (5.1)$$

where U_{rad} is the energy density of radiation in the rest frame of the electron and v is the velocity of electrons.

Now we can notice interesting fact. If we compare Eq.5.1 with the expression for synchrotron power (Eq.4.15) we see that they both have the same electron-energy dependence $\propto E^2$ ($\propto \gamma^2$), so their effects on radio spectra are indistinguishable.

The ratio of the total amount of energy liberated by synchrotron radiation and by inverse Compton scattering by the same distribution of electrons is:

$$\frac{P_{\text{syn}}}{U_{\text{IC}}} = \frac{U_{\text{B}}}{U_{\text{rad}}} = \frac{B^2}{8\pi U_{\text{rad}}}, \quad (5.2)$$

where B is the magnetic flux density in the source region.

5.1 Inverse Compton scattering on CMB photons

The source of the low-energy photons might be the cosmic microwave background (CMB) photons with (for zero redshift) temperature 2.7 K and energy density $2.6 \times 10^{-5} \text{ eV m}^{-3}$. Of course, the distribution of CMB photons is isotropic.

We can introduce *the effective magnetic field* for inverse Compton losses B_{IC} . If we assume that $U_{\text{rad}} = B_{\text{IC}}^2/8\pi$ and the energy density of the radiation depends on the redshift as follows:

$$U_{\text{rad}} \propto (1+z)^4, \quad (5.3)$$

Then all together we get:

$$B_{\text{IC}} \approx 3.2 \times (1+z)^2 \mu\text{G}. \quad (5.4)$$

Manifestation of this phenomenon is the *Sunyaev-Zel'dovich effect*. That is inverse-Compton scattering of CMB photons by electrons in the hot intergalactic medium in clusters of galaxies produces detectable changes in the CMB spectrum. Observed distortions of the cosmic microwave background spectrum are used to detect the density perturbations of the universe. This is of profound importance in cosmology.

For the purposes of my thesis more important is another astrophysical phenomenon featuring inverse Compton scattering. It is believed that this is the source of production of high-energetic photons in the hot spots and the extended structures of double radio sources, [14] (see figure 3.3).

Chapter 6

Spectral ageing

Synchrotron theory predicts a break in a spectrum due to the radiative losses, which drifts in time. As a result of this fact we can infer the age of the source of synchrotron emission from its spectrum [43].

6.1 The model of an active phase

While the AGN is in an active phase, it supplies the energy to electrons from *central engine* into the galactic nucleus. The energy is transported by jets to extended components (lobes, tales or bridges). After that the electrons can live quite a long time inside the extended lobes, gradually losing their energy by emitting synchrotron photons in the magnetic field of the lobes and by inverse Compton scattering on CMB photons.

The spectrum can be described as synchrotron radiation and injection of a constant spectrum qE^{-p} combined with inverse Compton scattering on CMB photons. The model I am using is a modified version of the model called *continuous injection model*. It was first used by Kardashev [19]. The modification is the addition of the contribution of inverse Compton scattering (projected in Eq.6.3). The *kinetic equation* of electrons (this equation describes time evolution of a system of electrons) is then:

$$\frac{\partial N}{\partial t} = \beta \frac{\partial}{\partial E} (E^2 N) + qE^{-p}. \quad (6.1)$$

The kinetic equation consists of two parts. First one stands for synchrotron energy losses: $dE/dt = -\beta E^2$. For pure synchrotron losses (Kardashev's model):

$$\beta = bB_{\perp}^2, \quad (6.2)$$

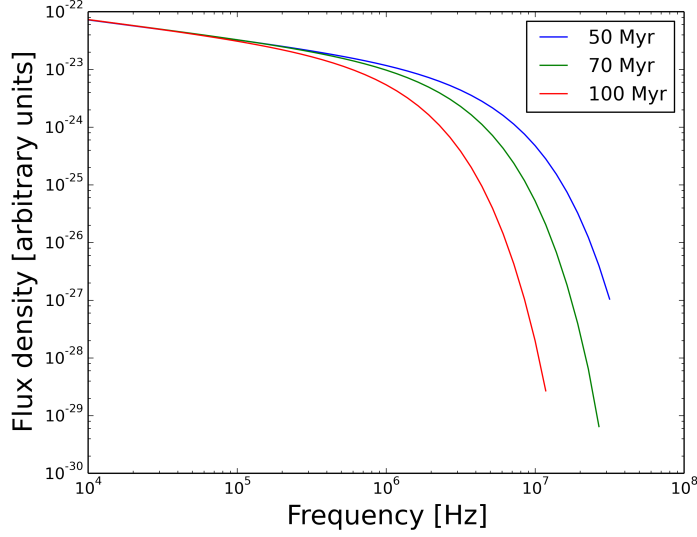


Figure 6.1: Assuming a constant magnetic field and no expansion, the total source age can be calculated from the break frequency. This model assuming infinitesimally short duration of the AGN activity episode.

where $b = 2.369 \times 10^{-3}$ But if we want to take into account also inverse Compton scattering on CMB then (according to [4]):

$$\beta(B, U_{\text{IC}}, \Theta) = c_2 H^2 (\sin^2(\Theta + \delta)), \quad (6.3)$$

where:

$$\delta = \left(\frac{B_{\text{IC}}}{B} \right)^2, \quad (6.4)$$

where B_{IC} is the effective magnetic field for inverse Compton scattering (Eq.5.4), B is the magnetic field of the source, $c_2 = 2.37 \times 10^{-3}$, [4].

Both the synchrotron losses (Eq.4.13) and inverse Compton scattering losses (Eq.5.1) are described by the law : $P \propto E^2$ ($E = \gamma m_0 c^2$). So from now on I can continue according to Kardashev's model only with corrected expression for β . Important consequence is that electrons with higher energy loss energy quicker and this is the reason why the age of a source is imprinted in its synchrotron spectrum (see figure 6.1).

The second part qE^{-p} accounts for the supply of energy to electrons from active central engine. Now we will proceed to find the form of the synchrotron

radiation.

First step is to find the solution of the kinetic equation (Eq.6.1). For electrons having the same pitch angle Θ the resulting distribution function is following:

$$N(E, \theta, t) = \frac{qE^{-(p+1)}}{\beta(p-1)} [1 - (1 - \beta t E)^{p-1}]. \quad (6.5)$$

The intensity of synchrotron radiation for the electrons making the same pitch angle θ is:

$$I_\nu(\alpha) = \frac{R}{4\pi} \int_0^\infty p(\nu, \theta, E) N(E, \theta, t) dE, \quad (6.6)$$

where R is the extent of the nebula along the line of sight and $p(\nu, \alpha, E)$ is the spectral distribution of radiation of a single electron (see Eq.4.17):

$$p(\nu, \theta, E) = CH_\perp F(\alpha), \quad C = 2.34 \times 10^{-22}, \quad \alpha = \frac{\nu}{\nu_c}, \quad (6.7)$$

where ν_c is the cut-off frequency (Eq.4.2).

By integration over a solid angle we finally get the intensity of radiation for given frequency:

$$I_\nu = \int_{4\pi} I_\nu(\theta) d\Omega. \quad (6.8)$$

In order to solve this, we will use the relation: $d\Omega = \sin\theta d\theta d\varphi$.

This model predicts a break in a spectrum ν_b which drifts in time as shown on figure 6.1. From this prospective we can say that the spectrum displayed on figure 3.4 is of a *zero age* source (with self-absorption part).

If we know the value of break frequency and the magnetic field B of a source (we assume that it is constant) we can get the time since the source formation t_{syn} in Myrs as follows:

$$t_s = 1610 \frac{B^{1/2}}{B^2 + B_{\text{IC}}^2} \frac{1}{[\nu_b(1+z)]^{1/2}}, \quad (6.9)$$

where B_{IC} is the effective magnetic field of the microwave background radiation (Eq.5.4).

For $\nu \ll \nu_b$ the spectrum has a power law shape $S(\nu) \propto \nu^{-\alpha_{\text{inj}}}$ with $\alpha_{\text{inj}} = (p-1)/2$. For $\nu \gg \nu_b$ the spectrum becomes steeper with $\alpha = \alpha_{\text{inj}} + 0.5$. This is shown on figure 6.2.

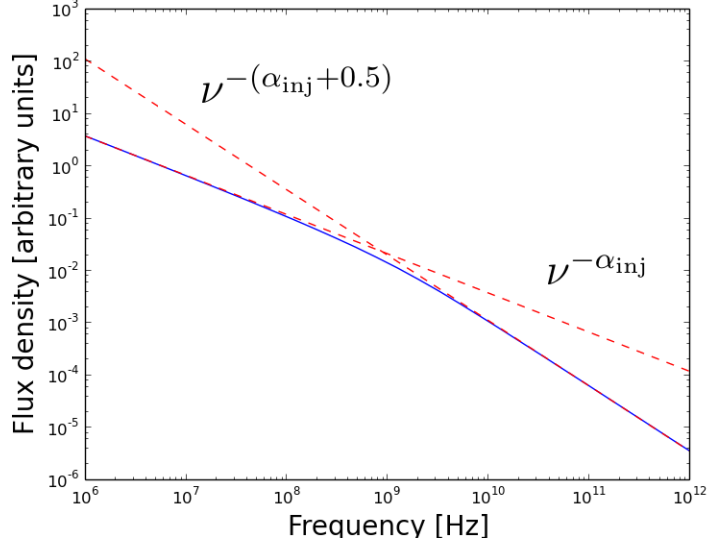


Figure 6.2: Modelled continuous injection synchrotron spectrum with parameters: $t = 30 \text{ kyr}$, $p = 2.5$, $H = 10^{-3} G$, $z = 0$.

6.2 The compact steep-spectrum and gigahertz peaked-spectrum radio sources

The term compact steep-spectrum sources (CSSs) and Gigahertz peaked-spectrum sources (GPSs) first appeared in the article from Peacock and Wall in 1983 [16].

They reported on *radio sources smaller than their optical host and not core dominated*. Their angular sizes are smaller than 2 arcsec (the corresponding projected linear sizes are typically $\leq 15 \text{ kpc}$) and they have steep radio spectra ($S \propto \nu^{-0.5}$) in the optically thin region. The spectrum may flatten in the MHz region in case of CSSs or peak in the GHz region in case of GPSs.

What is the connection between CSSs and GPSs and larger radio sources (if there is any)? Two scenarios have been proposed that would naturally explain the observed small sizes.

First is the *youth scenarion* [17]. As the title suggests it is based on idea that the observed small sizes are due to the early stage in the evolution of radio sources.

Second one is the *frustration scenarion* [18]. In this case it is assumed that the

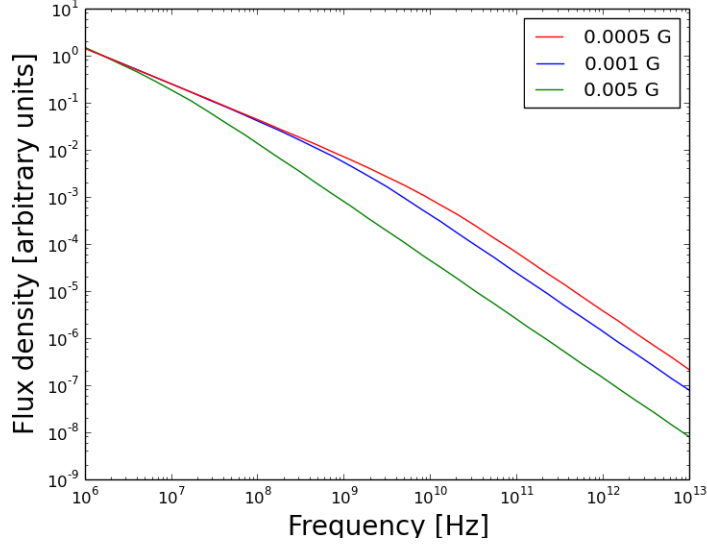


Figure 6.3: The dependence of the predicted spectrum on the strength of magnetic field ($t = 30$ kyr, $p = 2.5$).

source is placed in unusual interstellar medium of their host galaxies, for example a higher density. This prevents radio source from growing.

The spectra of these kinds of objects show non-thermal synchrotron origin of radiation. So we can try to estimate the ages (so called *radiative ages*) of these sources by applying the model of an active phase.

6.3 Radiative ages of CSSs

I chose sample of CSSs sources and I found corresponding spectra at CATS Database (Astrophysical CAtalogs support System). Where there was more observations for one frequency I averaged them with respect to errors of the measures.

The spectra were then fitted with the model of an active phase with two free parameters: t_s and α_{inj} . For fitting I used the Nelder-Mead method (simplex method) complemented in Python library SciPy package called *optimize*.

In order to determine the radiative ages from the model, the magnetic field B of the source has to be known. It is true that the inferred age depends strongly

<i>Name</i>	<i>Redshift</i>	B_{eq} 10^{-3} G
3C138	0.76	1.0
3C303.1	0.27	0.6
3C286	0.85	13
3C49	1.20	0.7
3C343.1	0.88	1.2
3C93.1	1.62	2.2

Table 6.1: The chosen CSSs sources and their physical parameters needed for the model, [23].

on magnetic field (as can be seen of fig.6.3). I took the values of B in the article from Murgia et. al ([23]). I used the so called *equipartition magnetic field* values.

This can be done under assumption that the radio sources contains relativistic particles and magnetic fields uniformly distributed and in *energy equipartition conditions* that means that energy density of the magnetic field is in equilibrium with the energy density of relativistic electrons. This combined with the fact, that synchrotron emission depends on both quantities we can (using Eq.4.15 (so N electrons with relativistic energy γ in a field B goes as $P \propto N\gamma^2 B^2$)) approximate that radiation at frequency ν comes from electrons with relativistic energy γ in a field B :

$$\nu \propto \gamma^2 B. \quad (6.10)$$

Equipartition assumption demands a minimum in the total energy (sum of the magnetic field energy and energy of electrons). From this we get the equipartition value of magnetic field:

$$B_{\text{eq}} \propto P^{-3/7} \nu^{-1/7}. \quad (6.11)$$

The parameters needed for the model for chosen sources are listed in table 6.1. According to many evidences, e.g.[20], the turnover in CSSs spectra are caused due to synchrotron self-absorption. I fitted just the optically thin regions of spectra (where $\tau \ll 1$, see figure 4.4). On figure 6.4 it is denoted as a dashed line. The results are shown on figure 6.4.

The optically thick parts might be fitted with the model of an active phase modified by low-frequency self absorption (see section 3.4) as follows ([4]):

<i>Name</i>	α_{inj}	t_s 10^3 yr
3C138	0.51	15.5
3C303.1	0.58	96.0
3C286	0.44	0.7
3C49	0.55	1.6
3C343.1	0.62	14.7
3C93.1	0.57	32.1

Table 6.2: The parameters inferred from best model fit of selected sources.

$$S(\nu) \propto \left(\frac{\nu}{\nu_1}\right)^{\alpha+\beta} \left(1 - \exp\left(\frac{\nu}{\nu_1}\right)^{-(\alpha+\beta)}\right) S_{CI}(\nu), \quad (6.12)$$

where ν_1 is the frequency at which the optical depth is equal to 1. In case of homogeneous synchrotron self-absorbed source $\beta = 2.5$ and α is the not aged spectral index in the frequency range where optical depth is much less than 1 (see figure 3.4).

The expression for ν_1 is according to A.Pacholczyk [4]:

$$\nu_1^{(s+4)/2} = c(s) H_{\perp}^{1/2} \frac{F_{\nu} \nu^{(s-1)/2}}{\Omega}, \quad (6.13)$$

where F_{ν} is the flux at a frequency ν at which the source is optically thin and Ω is angular size of the source in steradians, $c_{1,4}$ is a constant and it's value can be found in [4].

The parameters of the sources inferred from best fits are listed in table 6.2. It is clear that all the sources are according to this model very young (compare to the ages $\approx 10^7$ yr in frustration scenario). One of the questions remained is the legitimacy of using equipartition value of magnetic field. It can be partly justify by the fact that the B_{eq} does rather well for the low-frequency turnover in terms of synchrotron self absorption in many articles, e.g.[23], [20]. But of course this is not a proof for equipartition.

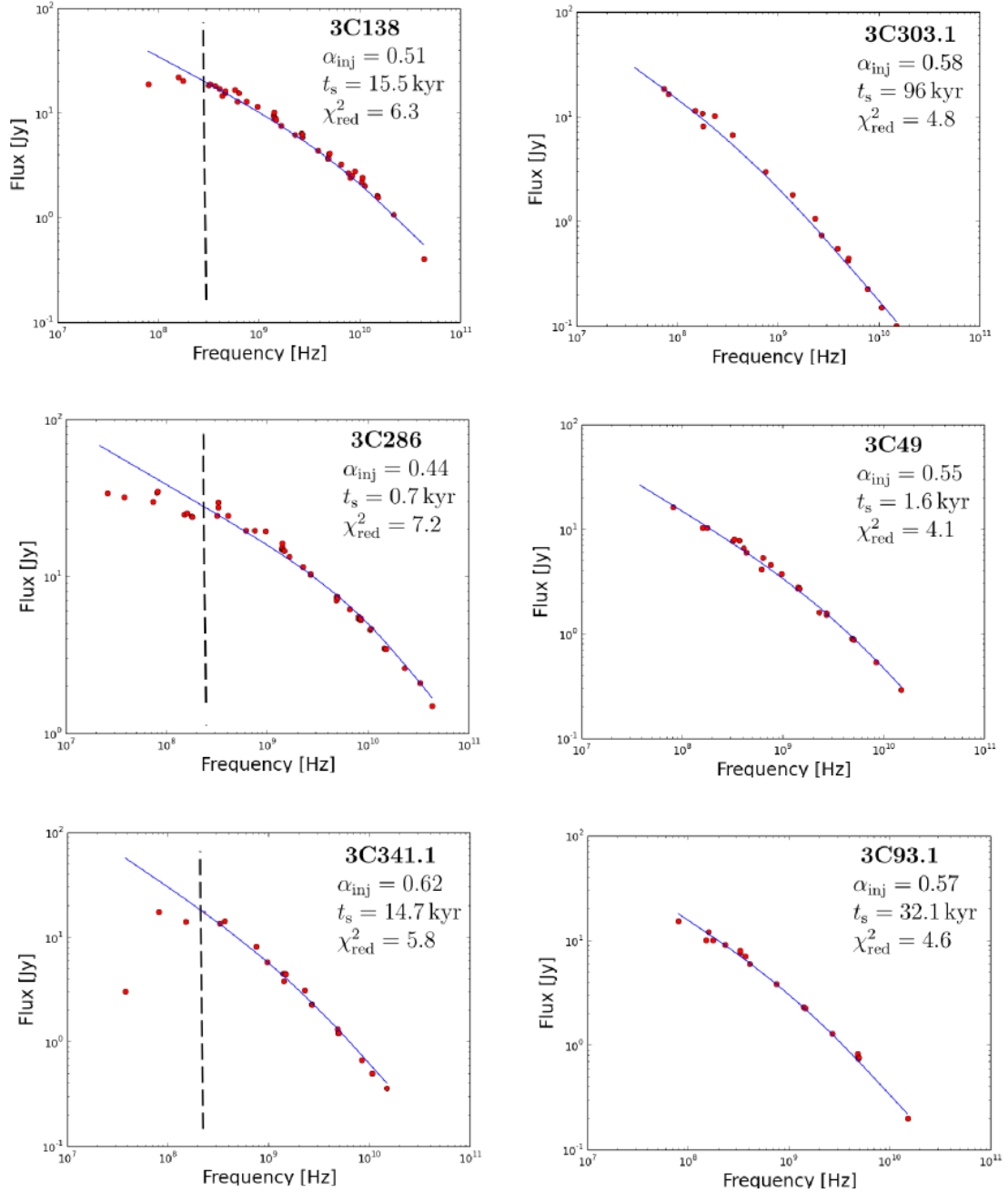


Figure 6.4: The spectra of selected sources fitted with the model of an active phase.

Chapter 7

Relic radio galaxies

There has been a growing body of evidence that AGN activity, which is powered by mass accretion onto a SMBH (see section 3.2), could be episodic. But the activity duty cycle is not yet fully understood. Such a knowledge would be crucial for understanding the influence of AGN on galaxy formation and evolution since we would be able to constrain the total energy output by AGN in the ISM and IGM.

Radio galaxies are ideal candidate to help us because their radio emission contains information about the history of AGN activity. In the cases when the AGN is not active or is restarted the remaining radio source is called *radio relic*.

7.1 Radio relic of young radio sources

As was discussed in section 6.2, CSSs and GPSs are thought to be young radio sources. But when we compare the number of known CSSs/GPSs and the number of observed large radio galaxies there is large discrepancy [22].

This leads to the prediction that some radio sources switch off soon after the birth leaving behind very small-scale radio relics, ([24].

We might be able to select such sources by constraints on their sizes (up to tens of kpc) and spectral indices of their spectra (section 7.3).

7.2 Restarted sources

If we assume that it is possible for radio galaxies to be active intermittently, we might be able to find fossil radio plasma left over from an earlier phase of

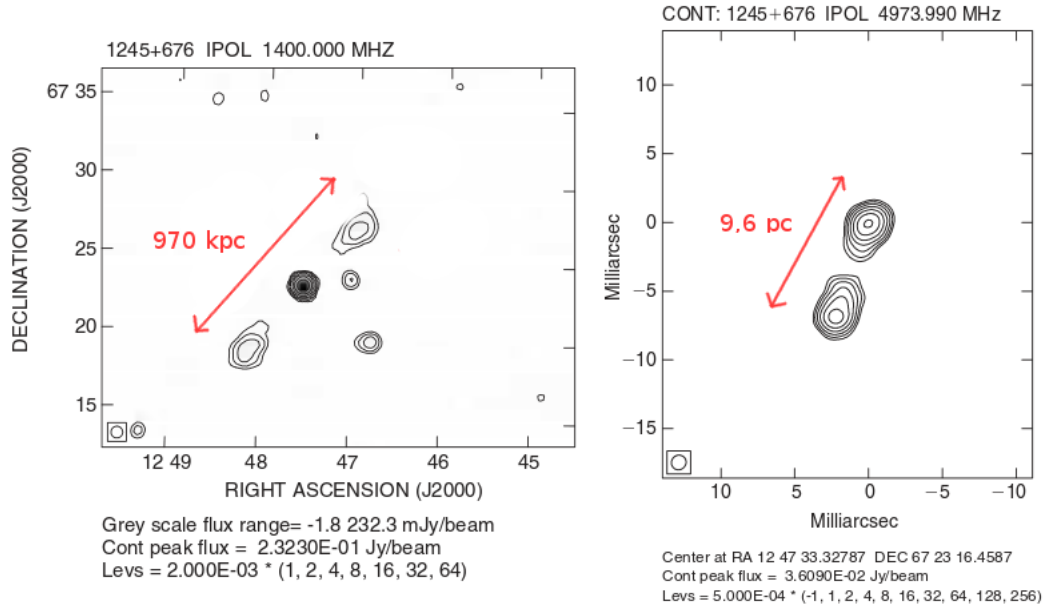


Figure 7.1: radio galaxy 1245+676, left NVSS image, right VLBI image, [25](modified) .

activity, while newly restarted core and radio jets are visible as well.

A very persuasive argument of episodic jet activity is so called double-double radio source. It is when we can see at the same time a new pair of radio lobes close to the nucleus and the *old* lobes more distant from the nucleus.

According to Marecki et al.([25]), an example of such an object is the radio galaxy 1245+676. It's outer structure (970 kpc) is five orders of magnitudes larger than the inner structure(9.6 pc).

7.3 Fading relics

In the fading phase the structures produced by continuing activity (radio core, jets and compact hot spots) are melting away. However, radio lobes still remain detectable with steep spectra ($s \sim 2$). Detecting these kind of sources is easier in lower frequencies. There are few known fading relics. This might be because we would need more sensitive instruments to detect them (see chapter 8). Another

explanation is possible that the time scale of AGN relics is short in comparison to the duration of the active phase.

7.4 The model of dying radio source

Once a radio loud AGN shuts down, there is no more energy supply from the core. The radio source is, poetically said, dying. In this phase we cannot observe structure directly connected to active sources (jets, hotspots) any more. But the ejected plasma can still be observed at lower frequencies. What we can observe is plasma being subject to radiative cooling only. The cooling is realized in form of synchrotron radiation (chapter 4) and inverse Compton scattering on CMB photons (chapter 5).

We can make following assumption to make the problem solvable (I follow the model proposed by Komisarov and Gubanov [21]):

1. Excluding any other form of cooling apart from the ones mentioned above.
2. The relativistic electrons do not escape from the radio lobes.
3. The radio lobes are uniform and the magnetic field distribution is isotropic.
4. No evolution of magnetic field strength.

Under these assumptions we can use model with following kinetic equation:

$$\frac{\partial N}{\partial t} = \beta \frac{\partial}{\partial E} (E^2 N) + q_0(t) q E^\gamma, \quad (7.1)$$

where

$$g(t) = \begin{cases} 1, & \text{for } 0 < t < t_0 \\ 0, & \text{for } t > t_0. \end{cases} \quad (7.2)$$

This part is simply taking into account a finite duration of the active phase t_0 . The distribution function $N(E, \Theta, t)$ is the solution of kinetic equation.

For $t < t_0$ (that means in an active phase) the solution is the same as for the active phase model (Eq.6.2).

After the injection has ceased (for $t > t_0$) the solution is:

$$N = \begin{cases} \frac{q_0 E^{-(p+1)}}{\beta(p-1)} ((1 - (t - t_0))^{p-1} - (1 - t_0)^{p-1}), & \text{for } E < \frac{1}{\beta t}; \\ \frac{q_0 E^{-(p+1)}}{\beta(p-1)} (1 - (t - t_0))^{p-1}, & \text{for } \frac{1}{\beta t} E \frac{1}{b(t-t_0)}; \\ 0 & \text{for } E > \frac{1}{b(t-t_0)}. \end{cases} \quad (7.3)$$

The coefficient $\beta(H, U_{\text{IC}}, \Theta)$ is the same as in Eq.6.3.

If we add one more assumption of pitch angle scattering of the electrons (due to interactions with plasma microturbulences) we can consider that the pitch angles are continually randomized and so the above expression is changed by the replacement $\sin^2 \alpha \rightarrow \langle \sin^2 \alpha \rangle = 2/3$. This assumption is used in the model of synchrotron losses from Jaffe and Perola [10].

Under mentioned conditions there appears new break in a spectrum ν_s , beyond which the spectrum drops exponentially:

$$\nu_s = \nu_b \left(\frac{t_s}{t_s - t_0} \right)^2, \quad (7.4)$$

where t_s is the total source age. So in the denominator there is the duration of the relic phase. This synchrotron model is described by two parameters:

- i) the lowest break frequency ν_b
- ii) the relic to total source age ratio $t_s/(t_s - t_0)$.

Another parameter can be the injection spectral index s_{inj} , which is related to p by Eq.4.21.

Before applying the model of the relic radio sources to real observations it is of course worth to take a look at the behaviour of the model depending on the parameters.

There is a predicted spectrum for $t = 1 \text{ Myr}$, $t_0 = 0.6 \text{ Myr}$, $B = 10^{-4} \text{ G}$ and $z = 0$ on figure 7.1. As can be seen on the figure, four asymptotic regions appears in the spectrum.

1. for $\nu \ll \nu_b(t)$ the spectrum has spectral index α_{inj} .
2. for $\nu_b(t) \gg \nu \ll \nu_b(t - t_0)$ the spectral index changes to $\alpha_{\text{inj}} + 0.5$.
3. for $\nu_b(t - t_0) \gg \nu \ll \nu_s(t - t_0)$ the spectral index changes to $4/3\alpha + 1$.
4. for $\nu \gg \nu_s(t - t_0)$ the spectral index drops exponentially.

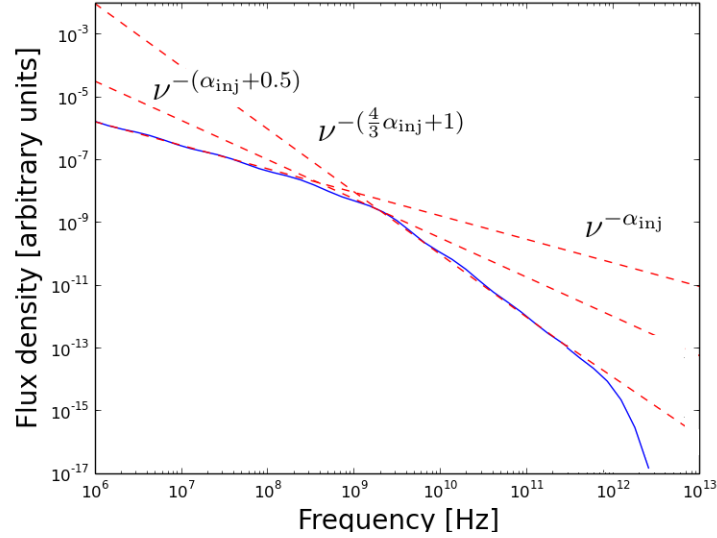


Figure 7.2: The predicted spectrum for parameters: $t = 1$ Myr, $t_0 = 0.6$ Myr, $p = 2.5$, $H = 10^{-4} G$, $z = 0$.

The variation of spectral index is illustrated on figure 7.2, where the value of spectral index was obtained by following expression:

$$s(\nu_1, \nu_2) = \frac{\log(S_1/S_2)}{\log(\nu_1/\nu_2)}. \quad (7.5)$$

What does cause this drop the fourth region with exponentially drop is clear?

According to [21], the high-frequency cut-off is caused by inverse Compton scattering losses of small pitch-angle electrons. These losses affect the anisotropy of the electron pitch-angle distribution and therefore the length of the last power law region with the spectral index $4/3\alpha + 1$.

On figure 7.4 there is shown the dependency of the model on the strength of magnetic field of the source. It is obvious that this dependency is very strong. From that we can assume that the asymptotic region with the spectral index $4/3\alpha + 1$ appears only if the magnetic field is strong enough. More precisely, if the magnetic field is roughly $B \geq 10^{-4} G$.

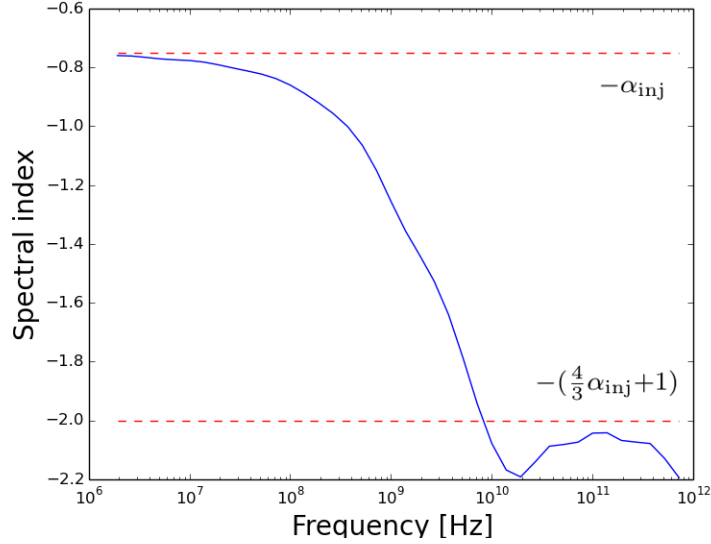


Figure 7.3: Spectral index variation for predicted spectrum from figure 7.1

7.5 The very steep spectrum radio sources

The very steep spectrum radio sources (VSSRSs) found in clusters of galaxies are believed to be relic radio galaxies whose nuclei have ceased their activity. These relics show no evidence of a core, jets or active hotspots. The unusually steep spectra ($\alpha - 2.0$) are explained by synchrotron losses of energy of relativistic electrons after the cessation of the injection of fresh particles into the radio source (explained in section 6.3). I chose sample of this kind of sources to fit them with the model described above.

7.6 Fitting the observed data with the model

It is of course important to test the model of dying radio source on real observations. To do it I chose few objects which are suspected to be the relic radio source due to their unusually steep spectra. As was mentioned before, there is a scarcity of such sources. Therefore I obtained data from *Parma et al.*, [26]. They searched throughout the whole WENSS catalogue (The Westerbork Northern Sky Survey) in order to find all the suspect sources. The sources I chose to study

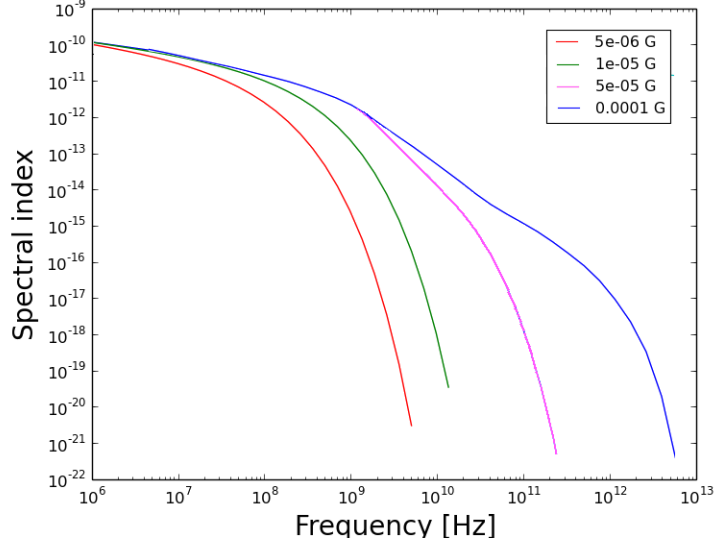


Figure 7.4: The dependence of predicted spectrum on magnetic field strenght B . Other parameters are fixed: t_0 : $t = 3$ Myr, $p = 2.0$, $z = 0$.

are listed in table 7.1 with the intrinsic parameters needed for the model.

As it was with the modelling of CSS spectra, the importance of the accurate value of the strength of magnetic field is very high, since the model shows strong dependence on it (figure 7.4). I used the equipartition value of B . Contrary to fitting CSS spectra, I decided to keep the value of spectral index fixed to $s_{\text{inj}} = 0.5$ that corresponds to $p = 2.0$. This value is characteristic for the spectra of jets and hot spots of many active radio sources. The reason was that it would be too many parameters for fitting spectra that has just few points.

The spectra were fitted with the model of dying radio source with two free

<i>Name</i>	<i>Redshift</i>	B_{eq} 10^{-6}G
WNB1438.0+3720	0.1	13.6
WNB0951.9+6037	0.2	8.8
WNB1257.4+3137	0.05	7.0

Table 7.1: The intrinsic parameters of chosen sources needed for the model,[26].

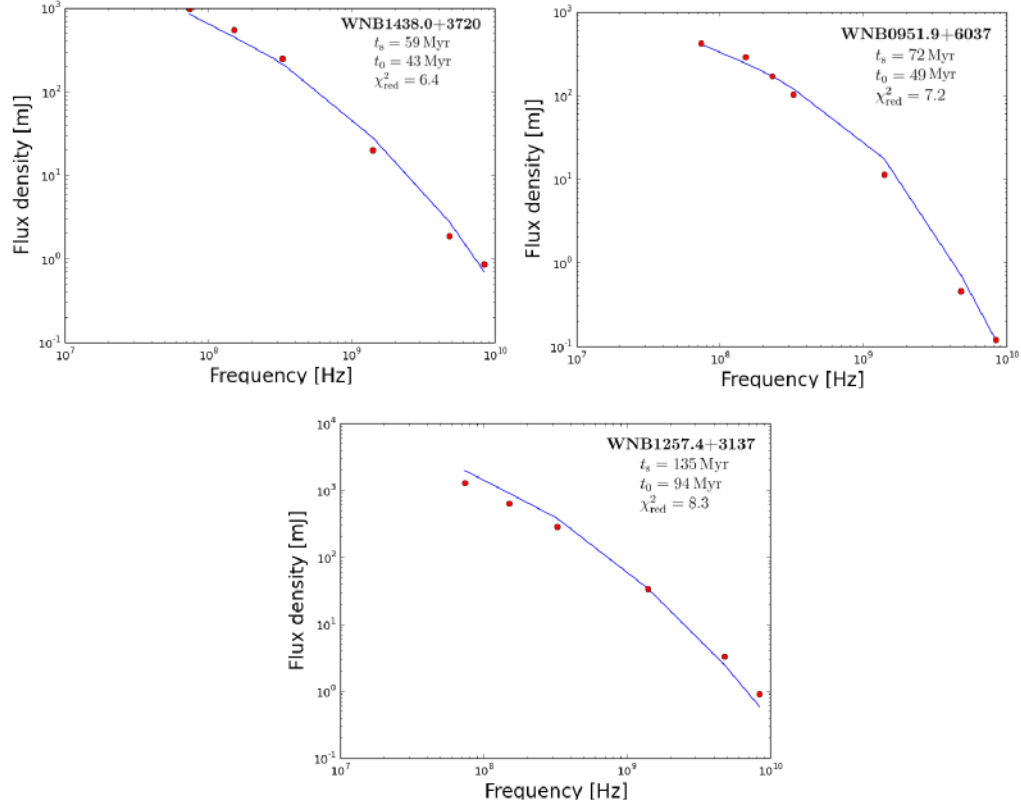


Figure 7.5: The spectra of selected sources with fitted model of dying radio source.

parameters: the total radiative age t_s and the duration of an active phase t_0 . For fitting I used the Nelder-Mead method (simplex method) complemented in Python library SciPy package called *optimize*. The results are shown on figure 7.5.

Even though the fits are not perfect I obtained reasonable results (table 7.2). The average age of the active phase t_0 is 63 Myr while the relic phase duration t_{off} is shorter with the average of 27 Myr.

The total radiative ages of dying radio sources from my sample has the average of 89 Myr. Compared to the average age of the *B2 sample* of radio galaxies (sample of 100 low luminosity radio galaxies) which is 16 Myr, the relics are no-

<i>Name</i>	t_s	t_0	t_{off}
	Myr	Myr	Myr
WNB1438.0+3720	59	43	16
WNB0951.9+6037	72	49	23
WNB1257.4+3137	135	94	41

Table 7.2: The parameters inferred from best model fit of selected sources.

table older. This justifies the using of term *dying* for these kind of galaxies. They are indeed likely in the last stage of radio sources. On the other hand, the ratio between the average of relic phase and active phase is 0.42 which does not really support the theory that the relic phase is much shorter than active phase and therefore we observe so little of them.

Chapter 8

LOFAR

So far we know of just a few relic radio sources especially compared to the observed population of AGN active radio sources. There are some possible explanations.

As was shown in chapter 7, radio relic's spectrum at low frequencies with steep declining towards higher frequencies. It follows that radio relics are brightest in low frequency radio maps. So one of the possible explanation is that our current instruments are not suitable for detecting such sources. To discover and explore more radio relics we need to improve our observational instruments in a sense of dynamic range and also they need to be more sensitive to low surface brightness. These demands are at least partially fulfilled with the new device called LOFAR.

8.1 Technical details

LOFAR is the Low-Frequency Array for Radio astronomy, built by ASTRON (the Netherlands Institute for Radio Astronomy). It has a modern design not using parabolic dishes but simple dipoles. It performs observations in the 10 MHz to 240 MHz frequency range with two types of antennas (Figure 8.2). Low Band Antenna is optimized for 0 – 80 MHz, whereas High Band Antenna is suitable for 120 – 140 MHz frequency band.

LOFAR is an interferometric array (see section 2.6) of about 20 000 antennas currently concentrated in 48 stations (more are in progress). The stations are spread around western and north Europe with 40 of them in the Netherlands. The total effective collecting area is approximately $300\,000\text{ m}^2$, depending on frequency and antenna configuration. The data processing is performed by a



Figure 8.1: on the left: a low-band antenna of LOFAR. On the right: a high-band antenna, [45].

supercomputer placed in the Dutch University of Groningen.

Sometimes LOFAR is called a *software telescope*. That means that the cost is not dominated by antennas itself, it is dominated by the cost of electronics. It has some unique properties for example its beam is variable unlike the beam of a classical dish radio telescope. LOFAR is the technological pathfinder for the Square Kilometre Array, a radio telescope project that will be built in Australia and South Africa (construction is scheduled to begin in 2018).

8.2 LOFAR on radio relics

Because of its frequency range reaching to low-frequencies, LOFAR is an ideal candidate for studying radio relics. With this instrument it will be possible to study not only the relics as a whole objects but to explore their parts separately making it possible to make age maps of these sources.

Indeed, some fresh views on restarted AGNs have been done already with LOFAR in 2015. For example, the ultra steep spectrum source VLSS J1431.8+1331 has been studied in order to estimate its duty cycle, [28].

Chapter 9

Conclusions

In first chapter of this thesis I briefly summarized the history and the important attributes of radio astronomy. Especially I tried to emphasize the differences between radio astronomy and astronomy in higher frequencies such as the role of the noise. I also described all the important quantities used later in the text.

Second chapter is dedicated to active galactic nuclei and their connection to formation and evolution of normal galaxies. In following section I explain the characteristics of synchrotron radiation and its connection to special relativity namely the interesting effect of beaming. Next is short description of inverse Compton scattering.

After these introductory parts I came to the crucial part of this thesis - models of radiative cooling of AGNs. First I dealt with an active phase of AGN, that means when there is still supply of energy from the central engine. The model predicts a break in a spectrum which drifts in time. So it is possible to use the model to estimate the age of a source. I chose sample of compact steep spectra sources to fitted them with the model. I obtained radiative ages of order $\sim 10^3$ years. These results are consistent with the youth scenario which states that the small sizes of CSS sources are due to the early stage of evolution.

Next I slightly changed the model in order to make it suitable for dying radio sources where the activity in the centre has ceased. Applying the model to the spectra of very steep spectrum radio sources I inferred their radiative ages of an active and shut off phase. The results indeed shows that these kind of sources (with average total age of 89 Myr) are older than the average radio galaxies (16 Myr). The average shut off phase duration is for my sample 27 Myr.

The studying of radio relics is a relatively young field. With new type of instruments such as LOFAR there will be plenty of new discoveries in near future.

Bibliography

- [1] RYBICKI, George B. a Alan P LIGHTMAN. Radiative processes in astrophysics. New York: John Wiley Sons, c1979, xv, 382 s. ISBN 0471827592.
- [2] LONGAIR, M. High energy astrophysics. 2nd ed. New York: Cambridge University Press, 1994-, v. <1-2>. ISBN 0521387736.
- [3] BURKE, Bernard F a Francis GRAHAM-SMITH. An introduction to radio astronomy. New York: Cambridge University Press, 1997, xii, 297 p. ISBN 052155604x.
- [4] PACHOLCZYK, A. [1970]. Radio astrophysics: nonthermal processes in galactic and extragalactic sources. San Francisco: W. H. Freeman.
- [5] GHEZ, A. M., S. SALIM, N. N. WEINBERG, J. R. LU, T. DO, J. K. DUNN, K. MATTHEWS, M. R. MORRIS, S. YELDA, et al. 2008. Measuring Distance and Properties of the Milky Way's Central Supermassive Black Hole with Stellar Orbits. *The Astrophysical Journal*. 689(2): 1044-1062. DOI: 10.1086/592738.
- [6] DRESSLER, Alan, Douglas O. RICHSTONE, N. N. WEINBERG, J. R. LU, T. DO, J. K. DUNN, K. MATTHEWS, M. R. MORRIS, S. YELDA, et al. 1988. Stellar dynamics in the nuclei of M31 and M32 - Evidence for massive black holes? *The Astrophysical Journal*. 324(2): 1044-1062. DOI: 10.1086/165930.
- [7] FERRARESE, Laura, David MERRITT, N. N. WEINBERG, J. R. LU, T. DO, J. K. DUNN, K. MATTHEWS, M. R. MORRIS, S. YELDA, et al. 2000. A Fundamental Relation between Supermassive Black Holes and Their Host Galaxies. *The Astrophysical Journal*. 539(1): L9-L12. DOI: 10.1086/312838.
- [8] GEBHARDT, Karl, Ralf BENDER, Gary BOWER, Alan DRESSLER, S. M. FABER, Alexei V. FILIPPENKO, Richard GREEN, Carl GRILLMAIR,

- Luis C. HO, et al. 2000. A Relationship between Nuclear Black Hole Mass and Galaxy Velocity Dispersion. *The Astrophysical Journal*. 539(1): L13-L16. DOI: 10.2172/839960.
- [9] MCCONNELL, Nicholas J., Chung-Pei MA, Karl GEBHARDT, Shelley A. WRIGHT, Jeremy D. MURPHY, Tod R. LAUER, James R. GRAHAM, Douglas O. RICHSTONE, Luis C. HO, et al. 2011. Two ten-billion-solar-mass black holes at the centres of giant elliptical galaxies. *Nature*. 480(7376): 215-218. DOI: 10.1038/nature10636.
- [10] JAFFE, W.J., PEROLA, G.C. Dynamical Models of Tailed Radio Sources in Clusters of Galaxies. *Astronomy and Astrophysics*, vol. 1973, no. 26, pp. 423.
- [11] THOMPSON, L. A., M. ISHIGURO, Craig LEVIN, Craig LEVIN a R. A. PERLEY. 1984. High resolution mm-VLBI imaging of Cygnus A. *The Astrophysical Journal*. 279: 109-116. DOI: 1504.01272.
- [12] MORGANTI, R., J. FOGASY, Z. PARAGI, T. a ORIENTI. 2013. Radio Jets Clearing the Way Through a Galaxy: Watching Feedback in Action. *Science*. 341(6150).
- [13] URRY, C. Megan, Paolo PADOVANI, Demosthenes KAZANAS, Peter GIOVANONI, Donald E. OSTERBROCK, Donald E. OSTERBROCK, Ian W. A. BROWNE a Neil JACKSON. 1995. Unified Schemes for Radio-Loud Active Galactic Nuclei. *Publications of the Astronomical Society of the Pacific*. 107: 618-636. DOI: 10.1007/978-3-642-77566-6_143.
- [14] SCHREIER, E. J., E. FEIGELSON, J. DELVAILLE, R. GIACCONI, J. GRINDLAY, D. A. SCHWARTZ a A. C. FABIAN. Einstein observations of the X-ray structure of Centaurus A - Evidence for the radio-lobe energy source. *The Astrophysical Journal*. 1979, 234: L39-. DOI: 10.1086/183105. ISSN 0004-637x.
- [15] SEYFERT, Carl K. (1943). "Nuclear Emission in Spiral Nebulae". *The Astrophysical Journal* 97: 28–40. DOI:10.1086/144488.
- [16] PEACOCK, J.A., WALL, J.V. 1982 — Bright extragalactic radio sources at 2.7 GHz. II - Observations with the Cambridge 5-km telescope. *Monthly Notices of the Royal Astronomical Society*, vol. 198, March, p. 843-860.

- [17] PHILLIPS, R., MUTEL, R.. On symmetric structure in compact radio sources. *Astronomy and Astrophysics*, vol. 1982, no. 106, pp. 21-24.
- [18] Van BREUGEL, W., MILEY, G., HECKMAN, T. 1984. Studies of kiloparsec-scale, steep-spectrum radio cores. I VLA maps. *Astronomical Journal*, vol. 89, pp. 5-22.
- [19] KARDASHEV., N. 1962. Nonstationarity of Spectra of Young Sources of Nonthermal Radio Emission. *Soviet Astronomy*, vol. 6, pp. 317.
- [20] VRIES, N. de, I.A.G. SNELLEN, R.T. SCHILIZZI a K.-H. MACK. Further evidence for synchrotron self-absorption from the CORALZ sample of young radio-loud AGN. DOI: 10.1002/asna.200811159. ISBN 10.1002/asna.200811159. Dostupné také z: <http://doi.wiley.com/10.1002/asna.200811159>
- [21] KOMISSAROV, S.S. a A.G. GUBANOV. Relic radio galaxies: evolution of synchrotron spectrum. *Astronomy and Astrophysics*. 1994, 285(5): 27-43.
- [22] O'DEA, Christopher P. a Stefi A. BAUM. Constraints on Radio Source Evolution from the Compact Steep Spectrum and GHz Peaked Spectrum Radio Sources. *The Astronomical Journal*. 113: 148-. DOI: 10.1086/118241. ISSN 00046256.
- [23] MURGIA, M. a C. FANTI et al. Synchrotron spectra and ages of compact steep spectrum radio sources. *Astronomy and Astrophysics*. 1999, 345: 769-777.
- [24] KAISER, C.R. Evolution of radio galaxies. *Astronomische Nachrichten*. 2009, 330(2-3): 270-274. DOI: 10.1002/asna.200811173. ISSN 00046337.
- [25] MARECKI, Andrzej, Peter D. BARTHEL, Antonis POLATIDIS, Izabela OWSIANIK, Jen-Hsuan HO, Nick DAWSON a Oliver DOUBLE. 2003. 1245 676 — a CSO/GPS Source being an Extreme Case of a Double-Double Structure. *Publications of the Astronomical Society of Australia*. 20(01): 200-215. DOI: 10.5040/9781408162811.
- [26] PARMA, P. a M. MURGIA. In search of dying radio sources in the local universe. *Astronomy and Astrophysics*. 2007, 470(8): pp.875-888.
- [27] Shul)SHULEVSKI, A., AGN relics in the radio sky : a LOFAR look into spectral ageing and AGN duty cycles. Doctoral thesis, 2015. 173 p.

- [28] SHULEVSKI, A., R. MORGANTI, P. D. BARTHEL, J. J. HARWOOD, G. BRUNETTI, R. J. VAN WEEREN, H. J. A. RÖTTGERING, G. J. WHITE, C. HORELLOU, et al. AGN duty cycle estimates for the ultra-steep spectrum radio relic VLSS J1431.8 1331. *Astronomy*. 2015, 583: A89-. DOI: 10.1051/0004-6361/201525632. ISSN 0004-6361.
- [29] flushleftNational Radio Astronomy Observatory. [online]. [cit. 2015-02-15]. <http://www.nrao.edu/whatisra/hist_jansky.shtml>
- [30] Le Repaire des Sciences. [online]. [cit. 2015-02-16]. Dostupné z: http://www.lerepairedessciences.fr/sciences/astronomie/-histoire/grote_reber.htm
- [31] The Vega Science Trust Videos . [online]. [cit. 2015-02-18]. <<http://www.vega.org.uk/video/programme/69>>
- [32] Image Gallery on NRAO. [online]. [cit. 2015-02-18]. <<http://images.nrao.edu/?id=321>>
- [33] Image Gallery on NRAO. [online]. [cit. 2015-02-18]. <2015-02-18].<http://images.nrao.edu/569>>
- [34] Wikipedia. [online]. [cit. 2015-04-12]. <http://en.wikipedia.org/wiki/Radi_owave/media/-File:Atmospheric_electromagnetic_opacity.svg>
- [35] William C. Keel's pages. [online]. [cit. 2015-06-10]. <http://www.astr.ua.edu/keel/agn/spectra.html>
- [36] Image Gallery on NRAO. [online]. [cit. 2015-05-12]. <<http://images.nrao.edu/501>>
- [37] Image Gallery on NRAO. [online]. [cit. 2015-05-12]. <<http://images.nrao.edu/132>>
- [38] Astronomy online. [online]. [cit. 2015-05-13]. <<http://astronomyonline.org/Science/RadioAstronomy.asp>>
- [39] ASTRON. [online]. [cit. 2015-05-22]. <https://www.astron.nl/mag/dokuwiki/lib/exe/fetch.php?media=radio_astronomy_lec_2_ma_garrett.pdf>

- [40] Wikipedia. [online]. [cit. 2015-05-24].
<<http://en.wikipedia.org/wiki/Directivity>>
- [41] BBC. [online]. [cit. 2015-05-24].
<http://www.bbc.co.uk/manchester/content/image_galleries/051007_lovell_telescope_gallery.shtml>
- [42] NRAO, [online]. [cit. 2015-02-21].
<<http://www.cv.nrao.edu/course/ast534/Interferometers1.html>>
- [43] ASTRON. [online]. [cit. 2015-12-21].
<<https://www.astron.nl/documents/conf/science/sci24w.pdf>>
- [44] CATS Database. [online]. [cit. 2015-12-27]. <<http://www.sao.ru/cats/>>
- [45] ASTRON. [online]. [cit. 2015-12-28]. <<https://www.astron.nl/>>

